ISSN 0031-0301, Paleontological Journal, 2006, Vol. 40, Suppl. 1, pp. S57–S89. © Pleiades Publishing, Inc., 2006.

New Upper Cambrian Trilobites from the Chopko River Section

A. I. Varlamov, K. L. Pak, and A. V. Rosova

Siberian Research Institute of Geology, Geophysics, and Mineral Resources, Krasnyi pr. 67, Novosibirsk, 630091 Russia

e-mail: geology@sniiggims.ru

Received January 12, 2005

Abstract—Six new genera, one new subgenus, and ten new species of trilobites are described from the Upper Cambrian Chopko Formation from a section of the Chopko River, Norilsk District, northwestern part of the Siberian Platform. These include one genus and two species of agnostids and five genera, one subgenus, and eight species of polymerids. The new taxa come from an interval of the section attributed to the upper two-thirds of the Upper Cambrian.

DOI: 10.1134/S0031030106070021

INTRODUCTION

Descriptions below resulted from partial treatment of the trilobite collection assembled by Varlamov, Pak, and Bragin in 1989. The locality, section, and association of sites with fauna are described in the paper by Varlamov *et al.* (2006, this issue). Therein, the terminology that is used for descriptions is given.

The trilobite material is housed in the Central Siberian Geological Museum (CSGM), United Institute of Geology, Geophysics, and Mineralogy, Siberian Branch of the Russian Academy of Sciences, Novosibirsk, collection no. 749.

SYSTEMATIC PALEONTOLOGY

CLASS TRILOBITA WALCH, 1771

Order Agnostida Salter, 1864

Family Diplagnostidae Whitehouse, 1936

Subfamily Pseudagnostinae Whitehouse, 1936

Genus *Pseudagnostus* Jakel, 1909

Subgenus *Pseudagnostus* (*Pseudagnostus*) Jakel, 1909

***Pseudagnostus* (*Pseudagnostus*) *intermedius* Pack, sp. nov.**

Plate 10, figs. 1–7

Etymology. From the Latin *intermedius* (intermediate).

Holotype. CSGM, no. 749/2, cephalon (**C**); northwestern Siberian Platform, Chopko River, outcrop Ch-8-I-2; Upper Cambrian, *Agnostotes* (*Pseudoglyptagnostus*) *clavatus–Irvingella perfecta* Zone, Chopko Formation (Pl. 10, fig. 2).

Diagnosis. **C** medium-sized, moderately convex, subovoid to subquadrate, with straight anterior margin with clear and deep median preglabellar furrow, border and border furrow both relatively narrow; glabella (**G**) elongated, with relatively large anteroglabella and slightly concave F3 transglabellar furrow, becoming shallower at axis. Pygidia (**Pyg**) semicircular, with very narrow third lobes on axis, relatively small axial node, and with border furrow broadening toward posterolateral corners and then narrowing toward posterior margin of **Pyg**. Posterolateral spines small, situated noticeably anterior to posterior end of axis; genae of **C** and pleural fields of **Pyg** with foveate-striated sculpture.

Description. **C** is medium-sized, 4.1–5.2 mm long, subovoid to subrectangular, having blunt rounded, almost straight anterior margin and straight posterior margins, moderately convex; acrolobes are very weakly compressed. **C** is 1.0–1.06 times as long as broad. The median preglabellar furrow is broad and deep, merging with the border furrow. The axial furrows (**SD**) are smoothed, distinct on casts and poorly expressed on carapaces, more clear in posterior halves and becoming shallower in anterior parts; they are narrower and shallower than the median preglabellar furrow. **G** is elongated, weakly convex, being most convex in the posterior part and flattening in the anterior part. **G** is 0.67–0.69 times as long as **C** and 1.93–2.12 as long as broad. The anteroglabella is flattened, semicircular, 0.28–0.32 as long as **G**, separated from the posteroglabella by a weakly concave, narrow, and shallow F3 transglabellar furrow, which is more distinct on its sides and becoming shallower axially, and is narrower and shallower than **SD**. The posteroglabella is weakly convex, 0.68–0.72 times as long as **G**; M3 divisions are ovoid, weakly convex, separated from M2 divisions by a very weakly expressed F2 furrow, which is narrow and shallower than **SD**; F2 furrows originate from **SD** halfway from the posterior end of **G**, developed abaxially and interrupted axially. The lateral sections of the F2 furrows are directed obliquely to the axis and forward. M3 divisions are separated by the axial node,

Plate 10

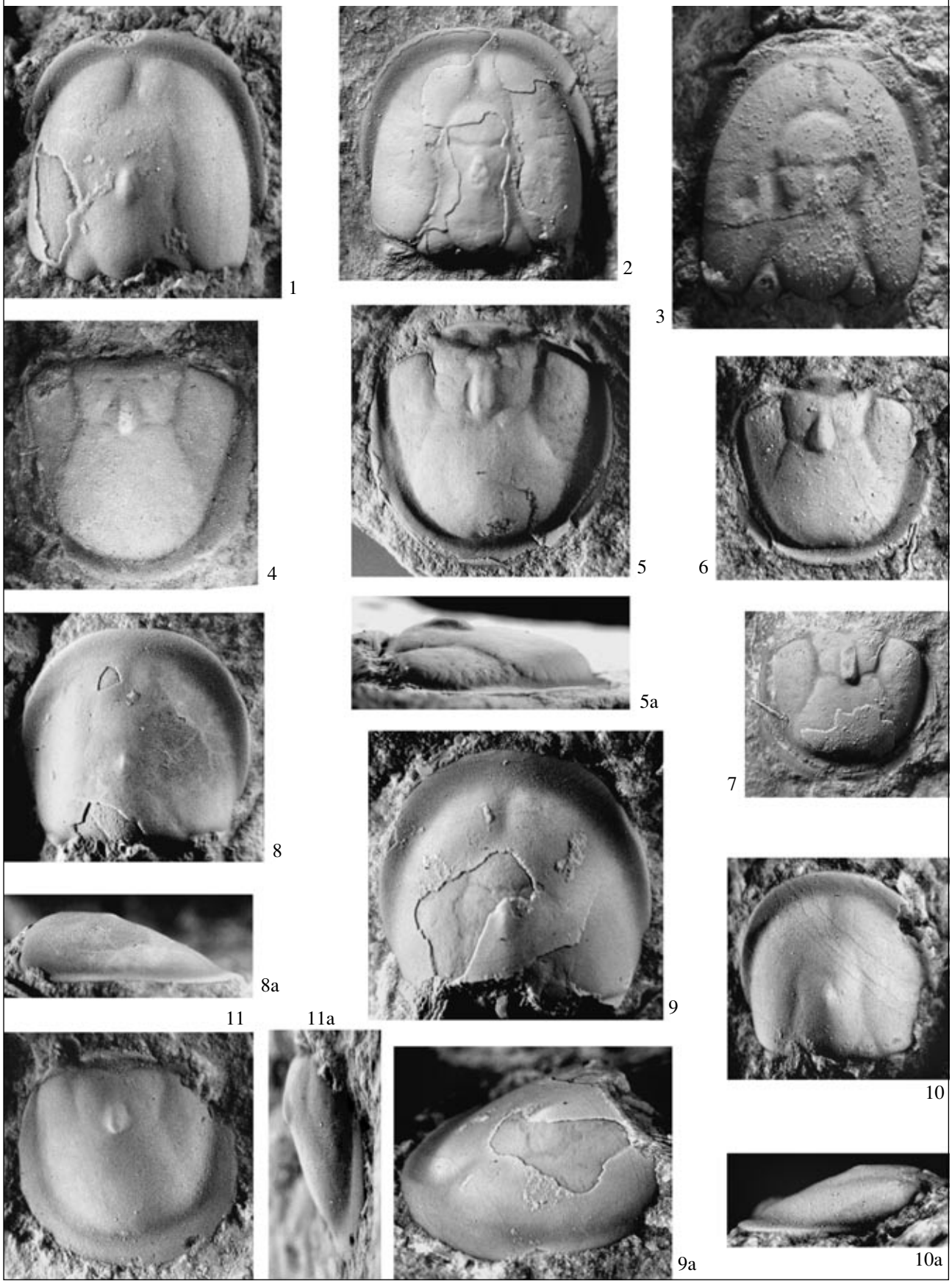

which forms a convex elongated ridge originating slightly behind the F3 transglabellar furrow and stretching toward the posterior end of **G** for 0.22–0.25 of the length of the latter. F1 of **G** are not developed. The maximum width of the posteroglabella is 0.34–0.37 times as great as the maximum width of **C**. The posterior end of **G** is rounded. The basal lobes are small, triangular, 0.21–0.22 times as long as **G**, the ratio of their maximum width to the maximum width of **C** is 0.17. **C** genae are weakly convex, sloping toward the sides and the anterior margin, the maximum width of the gena is 0.29 of the maximum width of **C**. The border of **C** is weakly convex, narrow, 0.047–0.049 times as wide as the **C**, forming thickened triangular areas with apices directed upward and slightly backward near the posterior ends of the genae. The border furrow of **C** is very narrow near the posterolateral corners, broadening toward the anterior margin of **C**, approximately as broad as the border, and as deep and as broad as the median preglabellar furrow. The surface of **C** is foveate-striated, the sculpture is more clearly expressed on casts and hardly noticeable on the exoskeleton.

Pyg is medium-sized or small, 2.9–4.9 mm long, moderately convex, semicircular to ovoid, with compressed acrolobes, weakly convex anterior and evenly rounded posterior margins, the ratio of the length of **Pyg** to its maximum width is 0.94–0.98. **SD** are moderately broad and deep in the anterior third, weakly converging backward to 0.3 of the axial length from the anterior margin of **Pyg**, where they rather abruptly, turn at an angle abaxially and run to the posterolateral corners, reaching the border furrow; the posterior parts of **SD** are narrower and shallower than the front ones. Near the border furrow, they become even shallower, becoming indistinct. The rachis is ax-shaped, with a straight anterior margin and a rounded posterior margin, moderately convex in its posterior part and weakly convex in its anterior part; it is 0.87–0.91 times as long as **Pyg** and 1.76–1.95 times as long as broad, the anteroaxis is 0.30–0.32 times as long as the axis, the posteroaxis is 0.68–0.70 times as long as the axis. The anteroaxis is subtrapezoid, weakly convex, flattened, weakly narrowing posteriad, with a concave anterior margin and a straight posterior margin, consisting of M1 and M2 divisions and very narrow small segments on each side of the axis, which can be treated as primordial or relict M3 divisions. M1 divisions are weakly convex, narrow, constricted near the axis, their length (longitudinal) is 0.1–0.12 of the axial length, they are separated from M2 divisions by a very shallow and narrow F1 furrow, which is distinct abaxially and interrupted near the axis, both parts of F1 furrow terminate in small pits, which are broader and deeper than adjacent areas of the inter-ring furrow; pits are situated on both sides of the axis. M2 division is subrectangular, weakly convex, flattened, its length (longitudinal) is much (two times) greater than the length of M1 division, whereas its width (transverse) is less than the width of M1 division; the length (longitudinal) of M2 is 0.2–0.24 the axial length. M2 is separated from M3 by a very narrow, shallow F2 furrow, which is as wide as but slightly deeper than F1, and considerably shallower and narrower than **SD**, distinct along the sides of the anteroaxis and interrupted at the axis; the lateral parts of F2 very faintly slope backward, almost transversely; on **Pyg** without exoskeleton, a pair of muscle scars is present in both M1 and M2, the scars are situated on each side of the axis, approximately one-quarter of the axis width apart; they are smaller on M1 and larger on M2. A ridgelike convex axial node stretches along the axis from M1, crossing M2 and running slightly over the posteroaxis; it broadens slightly backwards and is 0.27–0.33 times as long as the axis. A very narrow M3 division bordered posteriorly by a barely visible furrow F3 interrupted near the axial node is outlined behind M2. In the part of M3 adjacent to the axial node, a pair of small round notulae with small pits at the front margin is outlined. M3 divisions resemble similar structures in *Xestagnostus legirupa* Öpik, 1967 (p. 163, pl. 64, figs. 1, 2a, 2b, text-fig. 49). The posteroaxis is developed as a truncated circular sector, weakly convex in its anterior part and moderately convex in its posterior part; it is 0.67–0.7 times as long as the axis; the ratio of the maximum width of the posteroaxis to that of **Pyg** is 0.62–0.7, the ratio of the maximum and minimum widths of the posteroaxis is 1.71–1.94. A pair of

Explanation of Plate 10

Figs. 1–7. *Pseudagnostus* (*Pseudagnostus*) *intermedius* Pack sp. nov.: (1) paratype CSGM, no. 749/1, **C** with almost complete exoskeleton, outcrop Ch-24a-3, $\mathbf{a_1}$ of **C** = 4.3 mm, ×11; (2) holotype CSGM, no. 749/2, **C** with small fragments of exoskeleton, outcrop Ch-8-I-2, $\mathbf{a_1}$ of **C** = 4.1 mm, ×10; (3) specimen CSGM, no. 749/3, **C** without exoskeleton, outcrop Ch-19, $\mathbf{a_1}$ of **C** = 5.2 mm, ×10; (4) specimen CSGM, no. 749/6, **Pyg** without exoskeleton, outcrop Ch-18-10, $\mathbf{a_1}$ of **Pyg** = 4.3 mm, ×9; (5, 5a) paratype CSGM, no. 749/4, **Pyg** without exoskeleton, outcrop Ch-8-I-2, $\mathbf{a_1}$ of **Pyg** = 4.9 mm, ×9; (5a) lateral view, ×9; (6) specimen CSGM, no. 749/5, **Pyg** without exoskeleton, outcrop Ch-19, $\mathbf{a_1}$ of **Pyg** = 3.4 mm, ×10; (7) specimen CSGM, no. 749/7, **Pyg** with partially preserved exoskeleton, outcrop Ch-8-I-2, $\mathbf{a_1}$ of **Pyg** = 2.7 mm, ×10.

Figs. 8–11. *Pseudagnostus* (*Pseudagnostus*) *cryptus* Pack sp. nov.: (8, 8a) holotype CSGM, no. 749/8, **C** with almost complete exoskeleton, outcrop Ch-22a-II-1, $\mathbf{a_1}$ of **C** = 4.5 mm, ×8.5; (8a) lateral view, ×8.5; (9, 9a) paratype CSGM, no. 749/9, incomplete **C** partially without exoskeleton, outcrop Ch-24-II-1, $\mathbf{a_1}$ of **C** = 5.8 mm, ×7.5; (9a) frontolateral view, ×7.5; (10, 10a) specimen CSGM, no. 749/11, **C** with complete exoskeleton, outcrop Ch-24a-3, $\mathbf{a_1}$ of **C** = 3.3 mm, ×10; (10a) lateral view, ×10; (11, 11a) specimen CSGM, no. 749/12, **Pyg** with complete exoskeleton, outcrop Ch-24-II-1, $\mathbf{a_1}$ of **Pyg** = 3.8 mm, ×8.5, (11a) lateral view, ×8.5.

Figs. 2, 3, 5–7. Specimens from the *Agnostotes* (*Pseudoglyptagnostus*) *clavatus–Irvingella perfecta* Zone. Fig. 4. Specimen from the *Norilagnostus quadratus–Irvingella cipita* Zone. Figs. 1, 8–11. Specimens from the *Irvingella norilica* Zone.

rounded notulae arranged close to the pair of notulae on M3 division is developed along the axis near the anterior margin of the posteroaxis. Further back, there are two rows (seven pairs) of smaller notulae; these rows are weakly bent to the sides of **Pyg**. A small terminal node is situated on the axis at the posterior end of the rachis. The pleural fields of **Pyg** are weakly convex in the anterior parts and flattened in the posterior parts, wedging out toward posterolateral corners, the maximum width of the pleural field is 0.22–0.24 of the **Pyg** maximum width. The border is weakly convex, flattened, and narrow; its maximum width is 0.067–0.077 of the **Pyg** length. Near the anterior margin of **Pyg**, the border is convex, bent at an angle downward and slightly backward, separated from the pleurae by a narrow and deep (narrower and deeper than **SD**) part of the border furrow. The border furrow is relatively shallow and of uneven width, widening considerably from the anterolateral corners of **Pyg** toward the posterolateral corners and then narrowing again toward the posterior margin of **Pyg**. The maximum width of the border furrow is 0.07–0.077 of the **Pyg** maximum width. The border carries a pair of small posterolateral spines, which are situated at one-fifth of the axis length in front of its posterior end and directed backward and slightly abaxially. The arcular apparatus is glyptagnostoid (after Öpik, 1967), the facets are even and flat. The surface of **Pyg** is smooth, with grooves and pits in the pleural fields and on the lateral margins of the posteroaxis; these structures are extended to the border furrow.

Dimensions in mm and ratios:

Parameters	Specimen CSGM, no.		
	749/2	749/3	749/1
$\mathbf{a_1}$ of **C**	4.1	5.2	4.3
$\mathbf{b_{mx}}$ of **C**	4.1	4.9	4.3
$\mathbf{a_1}$ of **G**	2.8	3.6	2.9
$\mathbf{a_1}$ of anteroglabella	0.8	1.0	0.095
$\mathbf{a_1}$ of posteroglabella	2.0	2.6	2.05
$\mathbf{a_1}$ of basal lobes	0.6	0.8	0.7
b of anteroglabella	1.1	1.6	1.2
$\mathbf{b_{mx}}$ of **G**	1.4	1.7	1.5
b of basal lobes	0.7	0.8	0.7
$\mathbf{b_{mx}}$ of genae	1.2	1.4	1.2
$\mathbf{a_1}$ of axial node on **G**	1.1	1.6	1.3
a(**b**) of **C** border	0.2	0.25	0.2
a(**b**) of **C** border furrow	0.2	0.25	0.2
$\mathbf{a_1}$ of **C** : $\mathbf{b_{mx}}$ of **C**	1.0	1.06	1.05
$\mathbf{a_1}$ of **G** : $\mathbf{b_{mx}}$ of **G**	2.0	2.12	1.93
$\mathbf{a_1}$ of **G** : $\mathbf{a_1}$ of **C**	0.68	0.69	0.67
$\mathbf{a_1}$ of anteroglabella : $\mathbf{a_1}$ of **G**	0.29	0.28	0.32
$\mathbf{a_1}$ of posteroglabell : $\mathbf{a_1}$ of **G**	0.71	0.72	0.68
$\mathbf{b_{mx}}$ of **G** : $\mathbf{b_{mx}}$ of **C**	0.34	0.35	0.37
$\mathbf{a_1}$ of **C** border : $\mathbf{a_1}$ of **C**	0.049	0.048	0.047
$\mathbf{a_1}$ of basal lobes : $\mathbf{a_1}$ of **G**	0.21	0.22	0.24
$\mathbf{b_{mx}}$ of basal lobes : $\mathbf{b_{mx}}$ of **C**	0.17	0.17	0.17
$\mathbf{b_{mx}}$ of genae : $\mathbf{b_{mx}}$ of **C**	0.29	0.29	0.29
b of border furrow : **b** of border	1.0	1.0	1.0

Parameters	Specimen CSGM, no.		
	749/4	749/5	749/6
$\mathbf{a_1}$ of **Pyg**	4.9	3.4	4.3
$\mathbf{b_{mx}}$ of **Pyg**	5.0	3.9	4.6
$\mathbf{a_1}$ of axis	4.3	3.0	3.9
$\mathbf{a_1}$ of anteroaxis	1.5	0.9	1.25
$\mathbf{a_1}$ of posteroaxis	2.8	2.1	2.65
$\mathbf{b_{mx}}$ of axis	3.1	2.5	2.9
$\mathbf{a_1}$ of axial node on axis	1.4	0.8	1.2
a(**b**) of **Pyg** border	0.35	0.25	0.25
a(**b**) of border furrow on **Pyg**	0.25	0.15	0.15
a of M1 ring	0.5	0.3	0.4
a of M2 ring	1.0	0.6	0.8
$\mathbf{b_{mx}}$ of pleural fields	1.1	0.9	1.1
$\mathbf{a_1}$ of **Pyg** : $\mathbf{b_{mx}}$ of **Pyg**	0.98	0.94	0.94
$\mathbf{a_1}$ of axis : $\mathbf{a_1}$ of **Pyg**	0.87	0.88	0.91
$\mathbf{a_1}$ of anteroaxis : $\mathbf{a_1}$ of axis	0.30	0.30	0.32
$\mathbf{a_1}$ of posteroaxis : $\mathbf{a_1}$ of axis	0.7	0.7	0.68
$\mathbf{a_1}$ of M1 ring : $\mathbf{a_1}$ of axis	0.12	0.10	0.10
$\mathbf{a_1}$ of M2 ring : $\mathbf{a_1}$ of axis	0.24	0.20	0.20
$\mathbf{b_{mx}}$ of axis : $\mathbf{b_{mx}}$ of **Pyg**	0.62	0.64	0.63
$\mathbf{b_{mx}}$ of pleural fields : $\mathbf{b_{mx}}$ of **Pyg**	0.22	0.23	0.24
$\mathbf{a_1}$ of border : $\mathbf{a_1}$ of border furrow on **Pyg**	1.4	1.6	1.6
$\mathbf{a_1}$ of axial node : $\mathbf{a_1}$ of axis	0.33	0.27	0.31

Variability. Specimens examined demonstrate variation in the length-to-maximum width ratios of **G** (1.93–2.12) and of **C** (1.0–1.06); widths of border furrows and borders of **C** and **Pyg** vary within small ranges, as well as the ratio of the axis length to its anterior margin width (1.76–1.95). Additionally, the convexity of the posteroaxis changes slightly.

Comparison. The new species is intermediate between the *communis* and *cyclopyge* species groups (Shergold, 1977). Additionally, although the position of the axial node on **G** is similar to that defined by the term "spectaculate" (Shergold, 1975; Shergold *et al.*, 1990), it is close to that characterized by the term "papilionate" (ibid.).

The new species is very close to the species *Pseudagnostus* (*Sulcatagnostus*) (?) *dubius* Lu et Lin, 1989 (pp. 120, 236, pl. 15, figs. 10–12, China, western Zhejiang; Upper Cambrian, *Pseudoglyptagnostus clavatus–Sinoproceratopyge kiangshanensis* Zone). *Pseudagnostus intermedius* sp. nov. differs from *P.* (*S.*) (?) *dubius* in having a narrow M3 division, the broader and weakly narrowing backward anteroaxis (*P.* (*S.*) (?) *dubius* has an almost parallel-sided anteroaxis), in the

posterolateral spines of **Pyg** situated noticeably in front of the posterior end of the axis, in the evenly rounded posterior end of **Pyg** (according to the original description, the posterior end of **Pyg** is angular in *P.* (*S.*) (?) *dubius*, although the state of preservation of **Pyg** of the holotype illustrated in Pl. 15, fig. 12 does not allow making such a conclusion, in our opinion), in the considerably larger anteroglabella, almost straight and transverse anterior margin of **C** (narrowly rounded in *P.* (*S.*) (?) *dubius*), and in the presence of foveate-striated sculpture on the genae and pleurae. The great similarity of the pygidia of *P. intermedius* sp. nov. and the holotype of *P.* (*S.*) (?) *dubius* Lu et Lin suggests that they might be attributed to the same species. However, a small number of figured specimens of *P.* (*S.*) (?) *dubius* and their poor preservation does not allow a definite conclusion to be drawn, and, therefore, *Pseudagnostus intermedius* is here described as a separate species.

P. intermedius sp. nov. differs from *P. impressus* Lermontova, 1940 (Lermontova, 1940, p. 125, pl. 49, figs. 13, 13a; Kharaulakh; Upper Cambrian, lower half) in having a narrow M3 division on the axis, in the longer anteroglabella, less curved F3 transglabellar furrow, and in the presence of foveate-striated sculpture on the genae and pleural fields. Shergold (1977, p. 99) had originally attributed *P. impressus* to the *communis* species group, but he reclassified this species later, having assigned it to the *convergens* species group of the genus *Rhaptagnostus* Whitehouse, 1936 (Shergold, 1980, p. 36).

P. intermedius sp. nov. differs from *P.* (*Pseudagnostus*) *karatauensis* Ergaliev, 1980 (Ergaliev, 1980, p. 105, pl. 10, figs. 1–3, 5, 6; Kazakhstan, Lesser Karatau, Kyr-Shabakty River; Upper Cambrian, Sakian, *Glyptagnostus reticulatus* Zone) in having somewhat more laterally compressed **C**, longer anteroglabella, much more distinct median preglabellar furrow, and in the presence of M3 division on the axis.

The new species differs from *P.* (*Sulcatagnostus*) *rugosus* Ergaliev, 1980 (Ergaliev, 1980, p. 112, pl. 17, figs. 3, 4; Kazakhstan, Lesser Karatau, Kyr-Shabakty River; Upper Cambrian, Lesser Karatauan Stage, Zone *Agnostus scrobicularis*) in having a longer anteroglabella, more distinct median preglabellar furrow, and in the presence of M3 division on the axis.

P. intermedius sp. nov. differs from *P. "communis"* (Hall et Whitfield, 1877) (Pratt, 1992, p. 34, pl. 5, figs. 10–34; Canada, southern Mackenzie Mountains; Rabbitkettle Formation, Upper Cambrian, Steptoan and lower part of the Sanwaptan Stage) in having **C** more compressed laterally, in the presence of M3 division on the axis, in the border furrow, which expands toward posterolateral corners and then narrows again toward the posterior margin of **Pyg**, and in the position of the posterolateral spines noticeably in front of the posterior end of the axis.

Distribution. Upper Cambrian, *Agnostotes* (*Pseudoglyptagnostus*) *clavatus–Irvingella perfecta, Norilagnostus quadratus–Irvingella cipita, Irvingella norilica* zones.

Locality and Material. Ch-8-I-2: 2 **C** (well-preserved) and 3 **Pyg** (well and satisfactorily preserved); Ch-11-I-3: 1 **Pyg** (satisfactorily preserved); Ch-18-10: 1 **Pyg** (well preserved); Ch-19: 1 **C** (well-preserved) and 1 **Pyg** (well-preserved); Ch-22a-II-1: 2 **C** fragments (satisfactorily preserved) and 1 **Pyg** (satisfactorily preserved); and Ch-24a-3: 1 **C** (well-preserved).

***Pseudagnostus* (*Pseudagnostus*) *cryptus* Pack, sp. nov.**

Plate 10, figs. 8–11, Plate 11, figs. 1–3

Etymology. From the Greek *cryptos* (hidden).

Holotype. 749/8, **C**; northwestern Siberian Platform, Chopko River, outcrop Ch-22a-II-1; Upper Cambrian, *Irvingella norilica* Zone, Chopko Formation (Pl. 10, fig. 8).

Diagnosis. **C** and **Pyg** heavily smoothed, weakly convex; **C** and **Pyg** border furrows broad, very shallow, merging with borders to form flat fields surrounding acrolobes. **C** with weakly compressed acrolobes, median preglabellar furrow smoothed but discernible, **G** and genae forming single surface evenly sloping toward anterior margin of **C**. **Pyg** possessing compressed acrolobes, smoothed **SD**; axis weakly convex, with undivided anteroaxis, forming with pleural fields single weakly convex surface gently descending toward posterior margin of **Pyg**. **C** and **Pyg** surfaces smooth, with weak striae and pits on casts, which almost unexpressed on exoskeleton.

Description. **C** is medium-sized, 3.3–4.5 mm long, semicircular, with very evenly rounded anterior and posterior margins, weakly convex, strongly smoothed, 0.94–0.96 times as long as broad; the median preglabellar furrow is recognizable but poorly expressed, rather broad and shallow. **SD** are strongly smoothed, narrow and shallow. **G** is weakly convex, elongated, with the rounded anterior and broadly angular posterior ends, 1.67–1.93 times as long as broad, and 0.6–0.64 times as long as **C**. The anteroglabella is relatively small, semicircular, 0.28–0.3 times as long as **G**, separated from the posteroglabella by a poorly expressed, generally straight F3 transglabellar furrow, which is narrower and shallower than **SD**. The posteroglabella is jug-shaped, broadest anteriorly, constricted at the level of F2 furrow and narrowing toward the posterior margin of the **C**, terminating in a broadly angular posterior end. F2 furrows are very weak, barely noticeable, directed obliquely anterointernally, interrupted near the axis, starting from **SD** at 0.48 of the glabellar length from its anterior end, narrower and shallower than **SD**. The F1 furrows are not expressed. Small, nar-

Plate 11

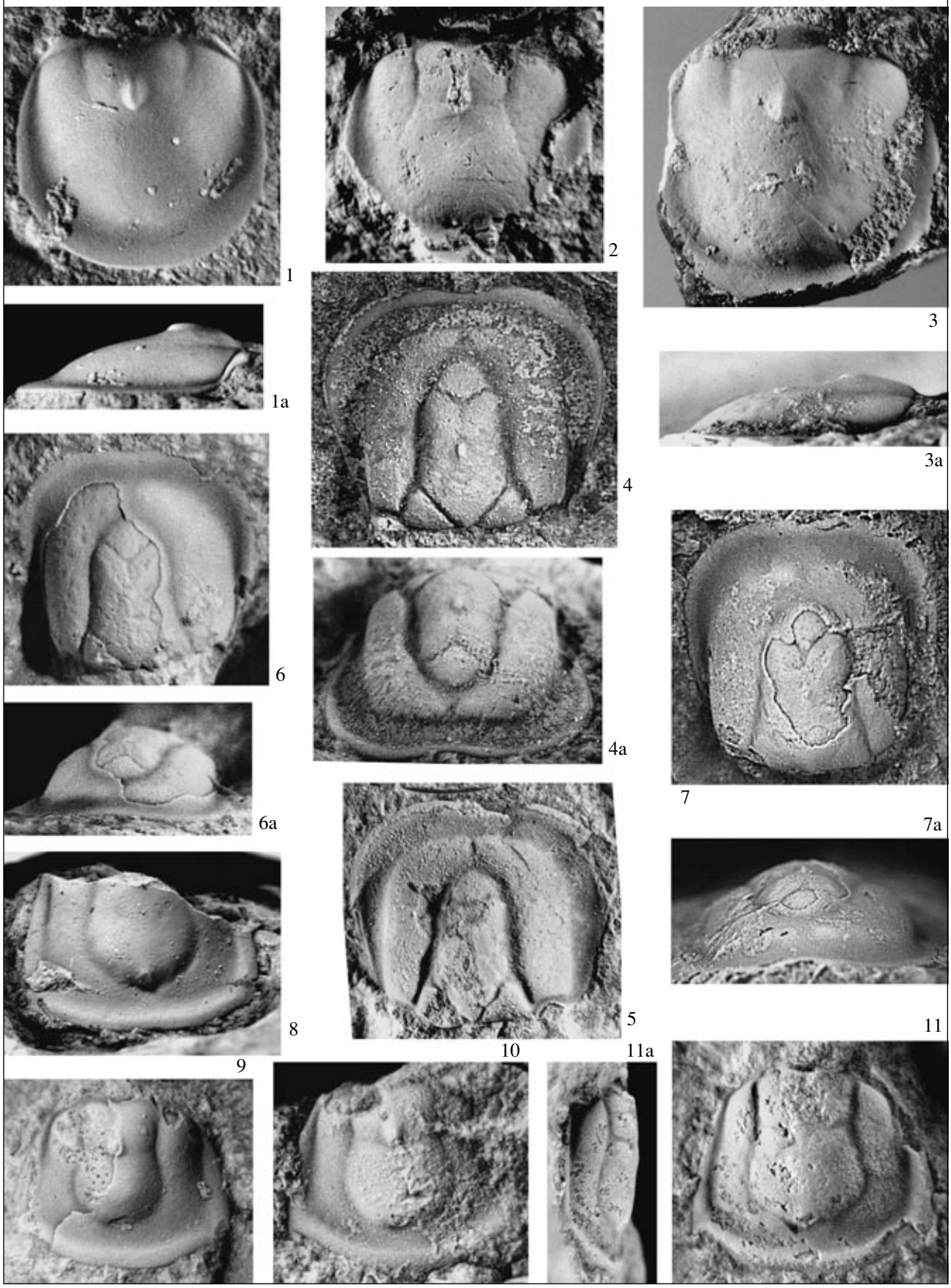

row, shallow furrows extend for approximately 0.15 of the glabellar length posterior to the F2 furrows and parallel to them; these small furrows are traceable abaxially but not expressed near the axis, directed obliquely outward and backward, not merging with **SD** but turning parallel to the latter and following the turnip-shaped undivided M1 and M2 divisions. A small and weakly elongated axial node with a ridgelike apex is developed at 0.45 of the glabellar length from its anterior margin. The axial node is situated clearly posterior to the F3 transglabellar furrow and a little anterior to, or partially at the level of F2 furrows, dividing the posterior parts of small, oval-shaped M3 divisions, which are 0.25–0.27 times as long as **G**. The basal lobes are small, simple, triangular, separated by narrow, shallow basal furrows, which are narrower and shallower than **SD**. The border of **C** is narrow and flat, merging with a broader and very shallow border furrow to form a single flat field, separated by a surface bend from the acrolobes. The length (longitudinal) of the border is 0.11–0.12 of the length of **C**. The genae of **C** are flattened, their maximum width is 0.27–0.31 of **C** maximum width, they narrow slightly near the axis. **G** with the genae form a single weakly convex surface sloping forward and abaxially. The surface of **C** is smooth and faintly foveate-striated.

Pyg are medium-sized and small, 3.8–4.3 mm long, strongly smoothed, with compressed acrolobes, weakly convex, semicircular, with a weakly convex anterior margin and an evenly rounded posterior margin. The ratio of the length of **Pyg** to its maximum width is 0.93–0.95. **SD** are smoothed, shallow, and relatively narrow in their anterior parts directed from the anterior margin of **Pyg** slightly obliquely backward and inward and outlining the anteroaxis. Much more smoothed, narrower, shallower, directed obliquely backward and outward posterior branches of **SD** are attached at an angle to the anterior parts of **SD** at 0.3 of the **Pyg** length from its anterior margin. The posterior branches of **SD** run to the border furrow. The axis is weakly convex, with a straight anterior margin and a rounded posterior margin, constricted in its anterior third, broadening considerably toward its posterior margin and reaching the border furrow; it is 0.85–0.87 times as long as **Pyg** and the ratio of its length to its maximum width is 1.31–1.35. A small terminal node surrounded by a circular depression is developed at the posterior end of the axis. F1 furrow is not expressed on the exoskeleton and entirely flattened out; F2 furrow is also smoothed and poorly developed on the exoskeleton. The anteroaxis is 0.33–0.35 times as long as the axis, the ratio of the maximum width of the anteroaxis to the maximum width of **Pyg** is 0.61–0.63. On casts, the F1 furrows are very faintly developed on the sides, interrupted near the axis, the lateral parts are slightly beveled anteriorly; the F2 furrows are also developed on the sides of the axis, weakly beveled posteriorly, so that the M2 division is hexagonal; the length (longitudinal) of the M1 division is 0.12 of the axial length; the length (longitudinal) of the M2 division is twice as great, and is 0.23 of the axial length. On casts, the axial node originates immediately from the M1 division, stretching posteriorly along the axis, broadening and slightly overlapping the posteroaxis. There are three pairs of muscle scars visible on casts; one pair is within the F1 lobe, the second one is within the F2 lobe, and the third pair is near the anterior margin of the posteroaxis; the scars are positioned close to the axial node on each of its sides. Two curved lines of notulae converging near the posterior margin of the axis extend from the third pair. The notulae are noticeable on casts and very poorly visible on the exoskeleton. The pleural fields are weakly convex, sloping abaxially, and 0.21–0.23 times as wide as the maximum width of **Pyg**. The pleural fields merge with the axis into a single weakly convex surface, sloping abaxially and gently lowering from the axial node toward the posterior margin of **Pyg**. The border furrow is very shallow, merging with the border into a single flat field framing the acrolobes and separated from it by a surface bend; the width of the border is 0.12–0.15 of the **Pyg** length. There is one pair of very small posterolateral spines at one-third of the length of **Pyg** in front of its posterior

Explanation of Plate 11

Figs. 1–3. *Pseudagnostus* (*Pseudagnostus*) *cryptus* Pack sp. nov.: (1, 1a) paratype CSGM, no. 749/13, **Pyg** with complete exoskeleton, outcrop Ch-24a-3, $\mathbf{a_1}$ of **Pyg** = 4.0 mm, ×10; (1a) lateral view, ×10; (2) specimen CSGM, no. 749/14, incomplete **Pyg** without exoskeleton, outcrop Ch-24-II-1, $\mathbf{a_1}$ of **Pyg** = 3.9 mm, ×10; (3, 3a) specimen CSGM, no. 749/10, incomplete **Pyg** with complete exoskeleton, outcrop Ch-24-II-1, $\mathbf{a_1}$ of **Pyg** = 5.8 mm, ×8.5, (3a) lateral view, ×8.5.

Figs. 4–11. *Norilagnostus quadratus* (Lazarenko) gen. nov.: (4, 4a) specimen CSGM, no. 749/15, **C** without exoskeleton, outcrop Ch-18-10, $\mathbf{a_1}$ of **C** = 5.6 mm, ×7.5, (4a) frontal view, ×7.5; (5) specimen CSGM, no. 749/16, **C** without exoskeleton, outcrop Ch-18-10, $\mathbf{a_1}$ of **C** = 5.2 mm, ×7.5; (6, 6a) specimen CSGM, no. 749/17, **C** with partially preserved exoskeleton, outcrop Ch-24-II-1, $\mathbf{a_1}$ of **C** = 4.6 mm, ×8.5, (6a) frontal view, ×8.5; (7, 7a) specimen CSGM, no. 749/18, **C** with partially preserved exoskeleton, outcrop Ch-24-II-1, $\mathbf{a_1}$ of **C** = 5.8 mm, ×7.8; (7a) frontal view, ×7.8; (8) specimen CSGM, no. 749/19, fragment of **Pyg** with exoskeleton, outcrop Ch-22a-II-1, $\mathbf{a_1}$ of **Pyg** = 2.5 mm, ×10; (9) specimen CSGM, no. 749/20, **Pyg** partially without exoskeleton, outcrop Ch-24a-3, $\mathbf{a_1}$ of **Pyg** = 2.8 mm, ×10.9; (10) specimen CSGM, no. 749/21, incomplete **Pyg** without exoskeleton, outcrop Ch-24a-3, $\mathbf{a_1}$ of **Pyg** = 3.6 mm, ×9.7; (11, 11a) specimen CSGM, no. 749/22, **Pyg** without exoskeleton, outcrop Ch-24-II-1, $\mathbf{a_1}$ of **Pyg** = 3.7 mm, ×10; (11a) lateral view, ×10.

Figs. 4 and 5. Specimens from the *Norilagnostus quadratus–Irvingella cipita* Zone, other specimens from the *Irvingella norilica* Zone.

margin. The surface of **Pyg** is smooth, the pleurae have foveate-striated sculpture, which is distinct on casts and poorly visible on the exoskeleton. The articulating apparatus is glyptagnostoid (Öpik, 1963, 1967).

Dimensions in mm and ratios:

Parameters	Specimen CSGM, no.	
	749/8	749/11
$\mathbf{a_1}$ of **C**	4.5	3.3
$\mathbf{b_{mx}}$ of **C**	4.7	3.5
$\mathbf{a_1}$ of **G**	2.9	2.0
$\mathbf{a_1}$ of anteroglabella	0.8	0.6
$\mathbf{a_1}$ of posteroglabella	2.1	1.4
$\mathbf{a_1}$ of basal lobes	0.6	0.45
b of anteroglabella	1.3	1.0
$\mathbf{b_{mx}}$ of **G**	1.5	1.2
b of basal lobes	0.8	0.6
$\mathbf{b_{mx}}$ of genae	1.3	1.1
$\mathbf{a_1}$ of axial node	0.5	0.35
$\mathbf{a_1}$ of **C** border	0.5	0.4
$\mathbf{a_1}$ of **C** : $\mathbf{b_{mx}}$ of **C**	0.96	0.94
$\mathbf{a_1}$ of **G** : $\mathbf{a_1}$ of **C**	0.64	0.60
$\mathbf{a_1}$ of anteroglabella : $\mathbf{a_1}$ of **G**	0.28	0.3
$\mathbf{a_1}$ of anteroglabella : $\mathbf{a_1}$ of **G**	0.72	0.70
$\mathbf{a_1}$ of **C** border : $\mathbf{a_1}$ of **C**	0.11	0.12
$\mathbf{b_{mx}}$ of **G** : $\mathbf{b_{mx}}$ of **C**	0.31	0.34
$\mathbf{b_{mx}}$ of genae : $\mathbf{b_{mx}}$ of **C**	0.27	0.31
$\mathbf{a_1}$ of basal lobes : $\mathbf{a_1}$ of **G**	0.2	0.22
$\mathbf{b_{mx}}$ of basal lobes : $\mathbf{b_{mx}}$ of **C**	0.17	0.18

Parameters	Specimen CSGM, no.	
	749/12	749/13
$\mathbf{a_1}$ of **Pyg**	3.8	4.0
$\mathbf{b_{mx}}$ of **Pyg**	4.0	4.2
$\mathbf{a_1}$ of axis	3.3	3.4
$\mathbf{a_1}$ of anteroaxis	1.1	1.2
$\mathbf{a_1}$ of posteroaxis	2.2	2.2
$\mathbf{b_{mx}}$ of anteroaxis	1.7	1.8
$\mathbf{b_{mx}}$ of axis	2.5	2.6
$\mathbf{a_1}$ of **Pyg** border	0.5	0.6
$\mathbf{a_1}$ of axial node	1.3	1.5
$\mathbf{a_1}$ of M1 ring	–	–
$\mathbf{a_1}$ of M2 ring	–	–
$\mathbf{b_{mx}}$ pleural fields	0.9	0.9
$\mathbf{a_1}$ of **Pyg** : $\mathbf{b_{mx}}$ of **Pyg**	0.95	0.95
$\mathbf{a_1}$ of axis : $\mathbf{a_1}$ of **Pyg**	0.87	0.85
$\mathbf{a_1}$ of axis : $\mathbf{b_{mx}}$ of anteroaxis	1.98	1.96
$\mathbf{a_1}$ of anteroaxis : $\mathbf{a_1}$ of axis	0.33	0.35
$\mathbf{a_1}$ of **Pyg** border : $\mathbf{a_1}$ of **Pyg**	0.13	0.15
$\mathbf{b_{mx}}$ of anteroaxis : $\mathbf{b_{mx}}$ of **Pyg**	0.43	0.43
$\mathbf{b_{mx}}$ of R : $\mathbf{b_{mx}}$ of **Pyg**	0.63	0.61
b of pleural fields : $\mathbf{b_{mx}}$ of **Pyg**	0.23	0.21
$\mathbf{a_1}$ of M1 ring : $\mathbf{a_1}$ of axis	–	–
$\mathbf{a_1}$ of M2 ring : $\mathbf{a_1}$ of axis	–	–

Comparison. The species described differs from all know species of the genus *Pseudagnostus* Jakel in **C** and **Pyg** being strongly smoothed and weakly convex and in having broad and flat fields formed by merged borders and border furrows. *P. cryptus* sp. nov. is also distinguished by the fusion of **G** and the genae of the **C**, as well as the pleural fields and the axis of **Pyg** into single surfaces, which are gently sloping from the axial nodes toward the anterior margins of **C** and the posterior margins of **Pyg**.

Remarks. A cast of **Pyg** of the holotype of *Ammagnostus integriceps* Öpik (1967, pl. 66, fig. 6a) from the *Glyptagnostus stolidotus* Zone of the Australian Middle Cambrian demonstrates a great similarity to **Pyg** of *P. cryptus* sp. nov. An essential difference is the position of the terminal node, which is situated much further from the posterior margin of the axis in *A. integriceps.* Additionally, although the posterior branches of **SD** of *P. cryptus* sp. nov. do not diverge very abruptly, the posteroaxis of its **Pyg** is much broader than in *A. integriceps.*

Distribution. Upper Cambrian, *Irvingella norilica* Zone.

Locality and Material. Ch-22a-II-1: 1 **C** (well-preserved); Ch-24a-3: 1 **C** and 1 **Pyg** (well-preserved); and Ch-24-II-1: 3 **Pyg** (well and satisfactorily preserved).

Family Incertae

Subfamily Quadrahomagnostinae Peng, 1992

Genus *Norilagnostus* Pack, gen. nov.

Etymology. From the city of Norilsk and the common agnostid suffix *agnostus.*

Type species. *Pseudagnostus quadratus* Lazarenko, 1966 (Lazarenko, 1966, p. 46, pl. 1, figs. 24–26, 28?, 29?, non fig. 27), northeastern Siberian Platform, Khoiguollakh Creek, tributary of the Olenek River in its lower reaches; Upper Cambrian, *Irvingella–Cedarellus felix* Zone.

Diagnosis. **C** moderately convex, broadening from base anteriorly. Anterior margin of **C** saddle-shaped, with parts along axis curving backward and upward (in frontal view). Acrolobes compressed, subquadrate. Border furrow of **C** strongly broadened near anterolateral corners of **C**, narrowing toward axis and even more strongly narrowing toward posterolateral corners of **C**. Border weakly convex, flattened. Anteroglabella rhomboid, separated from posteroglabella by

V-shaped F3 transglabellar furrow. Posterior margin of **G** angular, with small swelling or node at its very end. Basal lobes small, triangular. F2 furrow resembling transglabellar furrow on casts, whereas only its lateral parts expressed on exoskeleton. Median preglabellar furrow deep and broad on casts and smoothed out on exoskeleton. Genae noticeably narrowing at axis. Gena surface covered with radial striae and foveae distinct on casts and poorly expressed on exoskeleton. **Pyg** moderately convex, broadening backward, with weakly convex anterior margin and concave three-edged posterior margin. Acrolobes subtrapezoidal, compressed. Border relatively narrow and weakly convex. Border furrow shaped as surface bend, diffused. Axis weakly convex, constricted near M2 division, anterior margin of axis concave, posterior margin rounded angular; axis closely approaching border furrow. Posteroaxis weakly broadening backward, with large terminal node on its posterior end. Unclear longitudinal depression, probably relict of postaxial axial furrow, visible behind posteroaxis. Pleural fields narrowing toward posterior margin of **Pyg**, where they are separated by depression. Small backward directed, abaxially posterolateral spines developed near posterolateral corners of **Pyg**. Surface of **Pyg** with foveate-striated sculpture, weakly expressed on casts and barely visible on exoskeleton.

Species composition. Monotypic genus.

Comparison. The peculiarity of *Norilagnostus* gen. nov. is in the combination of the neoagnostoid **C** with the ammagnostoid **Pyg**. A similar, quite unusual combination is observed in another close genus *Quadrahomagnostus* Chu (or Zhu) 1959 (genotype *Homagnostus* (*Quadrahomagnostus*) *subquadratus* Chu, 1959, p. 55, pl. 1, figs. 21–24; Sun, 1989, p. 74, pl. 2, figs. 14–17; China, Liaoning; Kushan Formation, Middle Cambrian, *Blackwelderia* and *Drepanura* zones). **C** of *Norilagnostus* gen. nov. differs from that of *Quadrahomagnostus* Chu in its anterior margin being bent backward and, at the same time, upward near the axis, in having a larger subrhomboid anteroglabella, V-shaped F3 transglabellar furrow (F3 is strongly curved backward in *Quadrahomagnostus*), in the genae being noticeably narrowed at **C** axis, and in the foveate-striated sculpture of the genae. **Pyg** of *Norilagnostus* gen. nov. differs from that of *Quadrahomagnostus* in having a subpentagonal posteroaxis with the rounded angular posterior margin bearing a large terminal node (in *Quadrahomagnostus*, the posterior margin of the axis is rounded, and the terminal node is very small, poorly visible or even absent), in a longer anteroaxis, and in a narrower and less distinct border furrow. A certain resemblance to the new genus is shown by the genus *Ivshinagnostus* Ergaliev, 1980 (type species *Ivshinagnostus ivshini* Ergaliev, 1980 (Ergaliev, 1980, p. 66, pl. 13, figs. 1–3), Kazakhstan, Lesser Karatau, Kyr-Shabakty River; Upper Cambrian, Sakian, *Ivshinagnostus ivshini* Zone). *Norilagnostus* gen. nov. differs from *Ivshinagnostus* Ergaliev in having the median preglabellar furrow, the genae being strongly narrowed at the axis, noticeably broadened anteriorly **C** with its anterior margin being concave near the axis, in the longer axis of **Pyg** with the broadened posteriorly posteroaxis, unclear and diffuse border furrow, in the presence of a large terminal node on the posterior end of the axis, and in the presence of a depression separating the pleural fields behind the axis; additionally, **C** and **Pyg** of the new genus have weakly constricted acrolobes and foveate-striated surfaces of the genae and pleural fields.

Remarks. The genus *Neoagnostus* Kobayashi, 1955, especially species of the "*clavus*" group (sensu Shergold, 1977, p. 81), is very similar to the new genus in the structure of **C**. **C** of *Norilagnostus* gen. nov. differs from **C** of the above species group of *Neoagnostus* in being noticeably broadened anteriorly, in the presence of a more distinct median preglabellar furrow, broader border furrow, saddle-shaped anterior margin, and in the genae narrowing anteriorly.

Pyg of *Norilagnostus* gen. nov. is quite similar to those of the genus *Ammagnostus* Öpik, 1967 (genotype *Ammagnostus psammius* Öpik, 1967, p. 139, pl. 55, fig. 3, pl. 66, figs. 1–4, text-fig. 40; Australia, Queensland; Middle Cambrian, *Glyptagnostus stolidotus* Zone). The differences are as follows: in the new genus, the axis terminates short of reaching the border furrow of **Pyg** (in *Ammagnostus*, the axis reaches the border furrow); the terminal node is situated on the posterior end of the axis, whereas it is noticeably shifted anteriorly from the posterior end in *Ammagnostus*; the posterior margin of the axis is more angular; the **Pyg** is broadening posteriorly, trapezoid; the posterolateral spines are more caudal relative to the posterior end of the axis, and the posterior margin is three-edged in *Norilagnostus* gen. nov.

Distribution. Northeast of the Siberian Platform, basin of the Olenek River in its lower reaches; Upper Cambrian, *Irvingella–Cedarellus felix* Zone; northwestern Siberian Platform, Chopko River; Upper Cambrian, *Norilagnostus quadratus–Irvingella cipita, Irvingella norilica* zones.

***Norilagnostus quadratus* (Lazarenko, 1966)**

Plate 11, figs. 4–11

Pseudagnostus quadratus Lazarenko, 1966 (partim): Lazarenko, 1966, p. 46, pl. 1, figs. 24–26, 28?, 29?, non fig. 27.

Holotype. CSGM, no. 36/8907, **C**; northeastern Siberian Platform, Khoiguollakh Creek, left tributary of the Olenek River in its lower reaches; Upper Cambrian, *Irvingella–Cedarellus felix* Zone (figured by Lazarenko, 1966, pl. 1, fig. 24)

Diagnosis. See generic diagnosis.

Description. **C** is trapezoid to subquadrate, moderately convex, with saddle-shaped anterior and straight posterior margins, medium-sized, 4.6 to 5.8 mm long; the ratio of the length of **C** to its maximum width is 0.83–1.0. **G** is elongated, 0.72–0.73 times as long as **C**, with a rounded angular anterior margin

and an angular posterior margin. **SD** are distinct, narrow, deeper on casts and less clear on exoskeleton, converging anteriorly and merging near the anterior margin of **G** with a broader and deeper median preglabellar furrow, which is connected to the border furrow. **G** is subdivided by a V-shaped F3 transglabellar furrow into the anteroglabella and posteroglabella; F3 is narrower and shallower than **SD**. The anteroglabella is rhomboid, being broadest near the F3 transglabellar furrow. The posteroglabella is moderately convex, subdivided by a weakly distinct F2 furrow into M3 and M1–M2 divisions. The F2 furrow is much shallower and narrower than **SD**, curved anteriorly near the axis of **C**. M3 divisions are oval-shaped, contiguous along the axis. The M1–M2 division is pentangular, weakly broadening backward from the F2 furrow, becoming narrower at one-eighth of the length of **G** from its posterior margin and terminating in an angular posterior margin of **G**, where a small swelling resembling a node is formed. The axial node, the anterior part of which enters a bend of the F2 furrow, is situated in the anterior part of the M1–M2 division; this axial node looks like an elongated ridge and is 0.063 times as long as **G**. The ratio of the length of **G** to its maximum width is 1.78–1.83; the anteroglabella is 0.25 times as long as **G** and 0.33 times as long as the posteroglabella. The basal lobes are relatively small, weakly convex, triangular, 0.24–0.27 times as long as **G** and 0.48–0.50 as wide as the maximum width of **G**. The genae are moderately convex, becoming half as wide in front of **G**; the maximum width of the genae is 0.22–0.26 of the maximum width of **C**. The acrolobes are moderately convex, subquadrate, compressed. The border is weakly convex, relatively narrow, its width is 0.061–0.065 of the length of **C**. The border is very narrow and filiform near the posterolateral corners of **C**, gradually broadening toward the anterior margin of **C**, gently curving near the anterolateral corners toward the axis being positioned subnormally to it. The border weakly curves backward near the axis, the same part of the border curves slightly upward in frontal view. The border furrow is very narrow near the posterolateral corners of **C**, widely broadening anteriorly and slightly narrowing near the axis; the ratio of the maximum width of the border furrow to the maximum width of the border is 1.5–2.0. Thickened triangular parts of the border with their apices oriented upward and slightly backward are developed near the posterior ends of the genae. The surface of the exoskeleton is punctate-granulated, the surface of the casts is punctate-foveate; the genae are covered with radial grooves and pits, which are distinct on casts and weakly expressed on the exoskeleton.

Pyg is trapezoid, with weakly convex anterior and weakly concave three-edged posterior margins, moderately convex; the ratio of the length of **Pyg** to its maximum width is 0.67–0.78. **SD** are narrow, moderately deep, being deeper and broader on casts than on the exoskeleton. From the anterior margin of **Pyg**, they are directed slightly inward and backward; from the M2 division, they gently curve slightly outward and, then, at 0.4 of the length of **Pyg** from its posterior angle, turn again at a small angle back to the axis and merge on the axis at an obtuse angle. The axis is generally subrectangular, weakly constricted near the M2 division, slightly broadened in its posterior part, with a straight anterior margin and a rounded angular posterior margin. The axis is 0.77–0.81 times as long as **Pyg** and the ratio of the length of the axis to its maximum width is 1.37–1.43. The M1 division is narrow (longitudinally), separated from the M2 division by a weakly expressed F1 furrow, which is practically unrecognizable on the exoskeleton, weakly convex, its length (longitudinal) is 0.13 of the axial length; the M2 division is longer (longitudinally), 0.24 times as long as the axis, but narrower (transversely) than M1, weakly convex, separated from the posteroaxis by F2 furrow developed only abaxially, the lateral parts of which are weakly beveled backward and inwardly, being broader and deeper than F1 furrow but narrower and shallower than **SD**. Two pairs of rounded muscle scars with notulae of much smaller diameter in their centers are visible on each side of the anteroaxis near **SD**. The posteroaxis is subpentagonal, weakly broadening posteriorly from F2, sharply narrowing again at 0.4 of the length of **Pyg** from its posterior margin. The posterior margin of the axis is rounded angular, with a rather large terminal node. Behind the posteroaxis, a shallow depression connected to the border furrow is traceable within a short distance along the axis; this is probably a relic of the postaxial furrow. A relatively small ridgelike axial node slightly overlapping the posteroaxis is developed within the M2 division. A pair of scars similar to those on the M1 and M2 divisions and possessing similar notulae in their centers is situated in the anterior part of the posteroaxis very close to the F2 furrow along the axial node. Two weakly curved rows of 7 or 8 pairs of notulae run from the anterior margin of the posteroaxis backward. The pleural fields are rather convex near the anterior margin of **Pyg**, flattening out toward the posterolateral corners, beveled backward and abaxially, narrowing noticeably behind the posteroaxis; their maximum width is 0.15–0.19 of the maximum width of **Pyg**. The border is weakly convex and relatively narrow, its width is 0.095–0.11 of the length of **Pyg**. The border gradually expands from the anterior margin of **Pyg**, where it is very narrow, stretches backward and outward, forming almost straight sections to the posterolateral corners, where it turns to the axis rather sharply, at an angle. The posterior part of the border is weakly concave and three-edged: two sections adjoining the posterolateral corners, the length of which is 0.27 of the **Pyg** width, are orientated to the axis and slightly obliquely backward; the central section, the length of which is 0.45 of the **Pyg** width, is perpendicular to the axis and connected to the lateral sections at obtuse angles; the connections are smooth and rounded. Relatively small triangular spines directed backward and outward are present near the posterolateral corners of **Pyg**. The border furrow is

diffuse, tripartite, two sections along the sides of the pygidium are a little broader and deeper than **SD**, directed parallel to the sides backward and outward, turning to the axis at an angle near the posterolateral corners and coming into the third section of the border furrow, which is gently concave, subperpendicular to the axis, broader than but approximately as deep as the lateral sections; the border is as broad as the border furrow. The surface of **Pyg** is smooth or very finely punctate-granulated. The foveate-striated sculpture is weakly expressed on casts and almost invisible on the exoskeleton.

Dimensions in mm and ratios:

Parameters	Specimen CSGM, no.		
	749/15	749/18	749/17
$\mathbf{a_1}$ of **C**	5.6	5.8	4.6
$\mathbf{b_{mx}}$ of **C**	6.8	5.8	5.0
$\mathbf{a_1}$ of **G**	4.1	4.2	3.3
$\mathbf{a_1}$ of anteroglabella	1.0	1.2	0.9
$\mathbf{a_1}$ of posteroglabella	3.1	3.0	2.4
$\mathbf{a_1}$ of basal lobes	1.0	1.1	0.9
b of anteroaxis	1.3	1.4	1.2
$\mathbf{b_{mx}}$ of **G**	2.3	2.3	1.8
b of basal lobes	1.1	1.1	0.9
$\mathbf{b_{mx}}$ of genae **C**	1.5	1.4	1.3
a of axial node	0.5	0.5	–
$\mathbf{a_1}$ of **C** border	0.35	0.35	0.3
$\mathbf{a_1}$ of **C** : $\mathbf{b_{mx}}$ of **C**	0.83	1.0	0.92
$\mathbf{a_1}$ of **G** : $\mathbf{a_1}$ of **C**	0.73	0.72	0.72
$\mathbf{a_1}$ of anteroglabella : $\mathbf{a_1}$ of **G**	0.24	0.28	0.27
$\mathbf{a_1}$ of posteroglabella : $\mathbf{a_1}$ of **G**	0.76	0.72	0.73
$\mathbf{b_{mx}}$ of **G** : $\mathbf{b_{mx}}$ of **C**	0.34	0.40	0.35
$\mathbf{a_1}$ of **C** border : $\mathbf{a_1}$ of **C**	0.063	0.061	0.065
$\mathbf{a_1}$ of **G** : $\mathbf{b_{mx}}$ of **G**	1.78	1.82	1.83
$\mathbf{a_1}$ of basal lobes : $\mathbf{a_1}$ of **G**	0.24	0.26	0.27
$\mathbf{b_{mx}}$ of genae : $\mathbf{b_{mx}}$ of **C**	0.22	0.24	0.25

Parameters	Specimen CSGM, no.	
	749/20	749/22
$\mathbf{a_1}$ of **Pyg**	2.8	3.7
$\mathbf{b_{mx}}$ of **Pyg**	3.6	5.5
$\mathbf{a_1}$ of **R**	2.0	3.0
$\mathbf{a_1}$ of anteroaxis	0.9	1.1
$\mathbf{a_1}$ of posteroaxis	1.1	1.9
$\mathbf{a_1}$ of M1 ring	–	0.4
$\mathbf{a_1}$ of M2 ring	–	0.7
$\mathbf{b_{mx}}$ of anteroaxis	1.3	1.8
$\mathbf{b_{mx}}$ of axis	1.4	2.2
$\mathbf{a_1}$ of **Pyg** border	0.3	0.35
a of axial node of axis	0.4	0.45
$\mathbf{b_{mx}}$ of pleural fields	0.7	0.8

Parameters	Specimen CSGM, no.	
	749/20	749/22
$\mathbf{a_1}$ of **Pyg** : $\mathbf{b_{mx}}$ of **Pyg**	0.78	0.67
$\mathbf{a_1}$ of axis : $\mathbf{a_1}$ of **Pyg**	0.77	0.81
$\mathbf{a_1}$ of axis : $\mathbf{b_{mx}}$ of axis	1.43	1.37
$\mathbf{a_1}$ of anteroaxis : $\mathbf{a_1}$ of axis	0.45	0.37
$\mathbf{a_1}$ of **Pyg** border : $\mathbf{a_1}$ of **Pyg**	0.11	0.095
$\mathbf{b_{mx}}$ of anteroaxis : $\mathbf{b_{mx}}$ of **Pyg**	0.36	0.32
$\mathbf{b_{mx}}$ of axis: $\mathbf{b_{mx}}$ of **Pyg**	0.39	0.4
$\mathbf{b_{mx}}$ of pleural fields : $\mathbf{b_{mx}}$ of **Pyg**	0.19	0.15
$\mathbf{a_1}$ of M1 ring : $\mathbf{a_1}$ of axis	–	0.13
$\mathbf{a_1}$ of M2 ring : $\mathbf{a_1}$ of axis	–	0.24

Variability. **C** depicted in Pl. 11, figs. 4, 4a, and figs. 7, 7a, being similar in size, demonstrate certain differences in shape, degree of curvature of their anterior margins at the axis, and in the widths of their border furrows. Probably, they belong to different species or subspecies of *Norilagnostus* gen. nov. However, a final conclusion can only be made based on more material.

Comparison. This is the only species in this genus.

Remarks. Lazarenko (1966, pl. 1, fig. 24) chose a **C** as the holotype, when she described the species *Pseudagnostus quadratus.* **Pyg** assigned to this species comes from another sample, and is considered by us to belong to another species, *Pseudagnostus* sp. aff. *rajovopsis* Pratt, 1992 (Lazarenko, 1966, pl. 1, fig. 27).

Distribution. Northeastern Siberian Platform, Kyutyungde Depression, Khoiguollakh Creek, left tributary of the Olenek River in its lower reaches; Upper Cambrian, *Irvingella–Cedarellus felix* Zone; northwestern Siberian Platform, Chopko River; Upper Cambrian, *Norilagnostus quadratus–Irvingella cipita, Irvingella norilica* zones, Chopko Formation.

Locality and Material. Ch-18-10: 3 **C** (well and satisfactorily preserved); Ch-24-II-1: 4 **C** (well-preserved) and 2 **Pyg** (satisfactorily preserved); Ch-24a-5: 1 **Pyg** (satisfactorily preserved); and Ch-22a-II-1: fragment of **Pyg** (well-preserved).

Order Ptychopariida Swinnerton, 1915

Suborder Ptychopariina Swinnerton, 1915

Superfamily Olenoidea Burmeister, 1843

Family Pterocephaliidae Kobayashi, 1935

Subfamily Aphelaspidinae Palmer, 1960

Genus *Rybniites* Pack, gen. nov.

Etymology. From the Rybnaya River.

Type species. *Rybniites* (*Rybniites*) *spiculatus* sp. nov., northwestern Siberian Platform, Chopko River; Upper Cambrian, *Agnostotes* (*Pseudoglyptagnostus*) *clavatus–Irvingella perfecta* Zone, Chopko Formation.

D i a g n o s i s. Dorsum (**D**) elliptical, 5–6 cm long. **C** broadly semicircular, approximately 0.33 times as long as **D**; length of cranidium (**Cr**) equal or less than its width at palpebra (**Pal**). Arculum (**Ar**) convex, rarely, weakly convex and flattened. Anterior branches of facial sutures sharply diverging. Librigenae broad, with equal posterior and lateral borders; long genal spines developed at posterolateral corners. Thorax (**T**) consisting of 16 segments, with distinct fulcral lines gently arcuate outward. Axis of **Pyg** having 4 to 7 rings, posterolateral parts of borders of **Pyg** broadened into backward oriented triangles, serving as bases for a pair of rather large flattened spines.

C o m p a r i s o n and R e m a r k s. Among others, the subfamily Aphelaspidinae Palmer, 1960 includes three species groups possessing very similar **Cr**, which are often indistinguishable from one another, and absolutely different **Pyg**. Some researchers regard the considerable differences in the structure of **Pyg** as significant grounds for attributing two well-known species groups to separate genera, *Eugonocare* Whitehouse, 1939 and *Olenaspella* Wilson, 1956 (Wilson, 1956; Palmer, 1962, 1965; Pratt, 1992). According to an alternative point of view, the two above mentioned species groups and the newly described third group are united in a single genus, *Eugonocare* Whitehouse as the subgenera *Eugonocare* (*Eugonocare*) Whitehouse, *Eugonocare* (*Olenaspella*) Wilson, and *Eugonocare* (*Pseudeugonocare*) Peng (Peng, 1992).

New species described below from the section of the Chopko River are extremely similar to *Pseudeugonocare* Peng in the structure of their **Pyg**, and, in our opinion, should be assigned to the same species group. As for the taxonomic rank of these species groups, we follow Palmer and Pratt and treat *Eugonocare* Whitehouse and *Olenaspella* Wilson as separate genera, as well as the third group of species, which is regarded by us as a new genus, *Rybniites* gen. nov. Additionally, the species described demonstrate certain differences from members of *Pseudeugonocare* Peng in the structure of their **Pyg** and **Cr**; therefore, two subgenera *Rybniites* (*Rybniites*) gen. et subgen. nov. and *Rybniites* (*Pseudeugonocare*) Peng have been recognized within the new genus.

Species of *Rybniites* gen. nov. differ from representatives of the genera *Eugonocare* Whitehouse and *Olenaspella* Wilson in the presence of broadened posterolateral areas of the **Pyg** border, which serve as bases for a pair of rather robust spines, in the presence of 16 segments in the **T** (versus 12–13 segments in *Olenaspella* and, probably, *Eugonocare*), and in the sharply diverging anterior branches of the facial sutures.

D i s t r i b u t i o n. Russia, Kazakhstan, China, Canada, lower and middle parts of the Upper Cambrian, from the *Innitagnostus inexpectans–Proceratopyge* (*Proceratopyge*) *protracta* Zone to the *Agnostotes* (*Pseudoglyptagnostus*) *clavatus–Irvingella angustilimbata*, *Pseudagnostus* "*curtare*," *Agnostotes* (*Pseudoglyptagnostus*) *clavatus–Irvingella perfecta*, and *Norilagnostus quadratus–Irvingella cipita* zones and beds with *Proceratopyge rectispinata* and *Parabolinoides calvilimbata.*

Subgenus *Rybniites* (*Rybniites*) Pack, gen. et subgen. nov.

D i a g n o s i s. **Cr** with narrow palpebral area of fixigena (buccula, **Bcl**) constituting 0.2–0.25, 0.35 of **G** width in middle, with short frontal area (corona, **Cor**), 0.2–0.27 times as long as **Cr**; $\mathbf{a_1Ar : a_1A}$ = 0.6–1.5; axis of **Pyg** consisting of four rings, pleural fields consisting of 3 or 4 pairs of pleurae and ribs.

S p e c i e s c o m p o s i t i o n. *Rybniites* (*Rybniites*) *spiculatus* gen., subgen. et sp. nov. *Rybniites* (*Rybniites*) *corniformis* gen., subgen. et sp. nov. *Rybniites* (*Rybniites*) *borealis* (Lermontova, 1940), (Lermontova in *Atlas of Leading*…, 1940, p. 153, pl. 49, figs. 4, 4a, 4b, Kharaulakh, lower half of Upper Cambrian).

?*Rybniites* (*Rybniites*) *ludvigsensis* (Pratt, 1992) (partim) (p. 54, pl. 15, figs. 14, ?16, 17–21, 25, non figs. 15, 22–24, Canada, Mackenzie Mountains; Upper Cambrian, Steptoan, beds with *Proceratopyge rectispinata* and beds with *Parabolinoides calvilimbata*, Rabbitkettle Formation).

C o m p a r i s o n. Species of the subgenus *Rybniites* (*Rybniites*) subgen. nov. differ from representatives of the subgenus *Rybniites* (*Pseudeugonocare*) Peng in having very narrow **Bcl**, which compose 0.2–0.25 and in a single case 0.35 of the width of **G** in the middle; in the short **Cor**, which composes 0.2–0.25 of the length of **Cr**, in the ratio of the lengths of the anterior border and the frontal field varying from 0.6 to 1.5 (this ratio if less than 0.6 in *Rybniites* (*Pseudeugonocare*)), in the fewer number of rings of the **Pyg** axis (four rings in *Rybniites* (*Rybniites*) against five to seven rings in *Rybniites* (*Pseudeugonocare*)), in the lesser number of pleurae and ribs (three to four pairs in *Rybniites* (*Rybniites*) against five to six pairs in *Rybniites* (*Pseudeugonocare*)).

R e m a r k s. *Rybniites* (*Rybniites*) *borealis* (Lermontova, 1940) has somewhat broader **Bcl** than other species of this subgenus, which constitute approximately 0.35 of the width of **G** in the middle. With the discovery of additional material on this and other species of the subgenus *Rybniites* (*Rybniite*s) Pack, subgen. nov., the diagnosis of the subgenus will be supplemented and corrected.

"*Aphelaspis*" *ludvigsensis* Pratt, 1992 has **Cr** practically indistinguishable from **Cr** of *Rybniites* (*R.*) subgen. nov. species (Pratt, 1992, pl. 15, figs. 14, 17–21, 25), whereas **Pyg** attributed to the same species (Pratt, 1992, pl. 15, figs. 15, 22–24) are closely similar to **Pyg** of *Origmaspis* (*Parbolinoides*) *calvilimbata* Westrop (Pratt, 1992, pl. 10. figs. 18, 21, 22). In addition, **Pyg** of both species have been found in the same collection K258. In Pratt's opinion, the only difference between **Pyg** of *O.* (*P.*) *calvilimbata* and that of *A. ludvigsensis*

is in the presence of faint interpleural furrows on the anterior pair of pleurae of *O.* (*P.*) *calvilimbata* ("The presence of a faint interpleural furrow in the anteriormost pleura separates pygidia of this species from those of *Aphelaspis ludvigsensis* n. sp. with which it occurs," Pratt, 1992, p. 48). It is evident that this character depends entirely on the preservation of particular specimens; moreover, such furrows can also be recognized on **Pyg** of "*A.*" *ludvigsensis* (Pratt, 1992, pl. 15, figs. 22–24). "*A.*" *ludvigsensis* Pratt has been provisionally included in the subgenus *Rybniites* (*Rybniites*) subgen. nov. until the type of **Pyg** characteristic of this species is established.

Distribution. Canada, Mackenzie Mountains; Upper Cambrian, Steptoan, beds with *Proceratopyge rectispinata* and beds with *Parabolinoides calvilimbata*, Rabbitkettle Formation; Russia, Northeastern Siberian Platform, Kharaulakh Mountains, lower half of the Upper Cambrian; northwestern Siberian Platform, Chopko River; Upper Cambrian, **A**gnostotes (*Pseudoglyptagnostus*) *clavatus–Irvingella perfecta, Norilagnostus quadratus–Irvingella cipita* zones, Chopko Formation.

***Rybniites* (*Rybniites*) *spiculatus* Pack, sp. nov.**

Plate 12, figs. 1–6

Etymology. From the Latin *spiculatus* (lance-shaped), after the form of the marginal spines on **Pyg**.

Holotype. CSGM, no. 749/23, **D**; northwestern Siberian Platform, Chopko River, **Ch-8-I-2**; Upper Cambrian, **A**gnostotes (*Pseudoglyptagnostus*) *clavatus–Irvingella perfecta* Zone, Chopko Formation (Pl. 12, fig. 1).

Diagnosis. Members of *Rybniites* (*Rybniites*) with marginal spines of **Pyg** lance-shaped and directed backward and slightly outward; $\mathbf{a_1}$ of **Ar** (longitudinally) : $\mathbf{a_1}$ of **A** = approximately 0.66–0.8.

Description. **D** are elongated elliptical, weakly convex, 32 and 43 mm long, with regular rounded anterior margins; **C** is 0.33 times as long as the **D**, the **T** is 0.53–0.55 times as long as the **D**, **Pyg** is 0.12–0.13 times as long as the **D**; **C** is broadly semicircular, weakly convex, the length of **C** is 0.5 of its maximum width.

Cr is subtrapezoid, with the broadly arcuate anterior margins and straight posterior margins, weakly convex; the length of **Cr** is 0.88–1.0 of its maximum width. The length of individual cranidia ranges from 1.9 to 15.7 mm. **G** is subcylindrical to subquadrate, weakly convex, very weakly narrowing forward, with a broadly rounded anterior margin and a straight posterior margin; the ratio of the length of **G** to its width in the middle is 1.03–1.21. The axial furrows (sulci dorsales, **SD**) are deep, straight, and narrow, very weakly converging anteriorly, sharply curving near the anterolateral corners of **G** to the axis, where they merge smoothly with the median preglabellar furrows (sulci preglabellares, **SPg**). Small fossulae, which are as wide as but slightly deeper than **SD**, are visible at junction points. The **SPg** is very gently arcuate forward, narrower and shallower than the **SD**, becoming shallower near the axis. **G** has three pairs of glabellar furrows (sulci glabellares, **SG**). $\mathbf{S_1G}$ are narrower and deeper than **SD**, originating at a small distance from them at 0.3 of the length of **G** from its posterior margin, very weakly geniculate, directed obliquely inward and backward; their inner ends are situated at 0.2 of the length of **G** from its posterior margin and at 0.4 of the width of **G** from **SD**. Furrows $\mathbf{S_2G}$ are narrower and shallower than $\mathbf{S_1G}$ or **SD**, originate at a small distance from the latter at 0.57 of the length of **G** from its posterior margin, are directed obliquely inward and backward, their inner ends are situated on the median line of **G** at 0.37 of the width of **G** base from **SD**. Furrows $\mathbf{S_3G}$ are poorly expressed, almost invisible, situated at 0.7 of the length of **G** from its posterior margin, very weakly beveled backward, short and almost transverse. The occipital furrow (sulcus occipitalis, **SO**) is weakly saddle-shaped, abaxially narrower and deeper than **SD**; rounded depressions (muscle scars) are visible in **SO** at 0.2–0.25 of the width of **G** base from **SD**; here, **SO** broadens and gently bends backward, becoming broader and shallower than **SD**; another pair of smaller muscle scars is present in **SO**, adjoining **SD**, but they are visible on large **Cr** only. The occiput (**O**) is almost parallel-sided, 0.2–0.27 times as long as **G**, with a weakly saddle-shaped anterior margin and an almost straight posterior margin. A small node is situated in the center of **O**. Additional furrows on lateral parts of **O** are observable in a number of **Cr**, mainly medium-sized and large **Cr** (over 8 mm long). The frontal area (corona, **Cor**) is weakly convex, sloping from **G** forward; $\mathbf{a_1Cor} : \mathbf{a_1G}$ = 0.35–0.38, $\mathbf{a_1Cor} : \mathbf{a_1Cr}$ = 0.21–0.24. The frontal field (area, **A**) is weakly convex, inclined forward and outward, 0.2–0.24 times as long as **G**. The anterior border furrow (sulcus arcularis, **SAr**) is distinct along the whole of its length, narrower and shallower than **SD**, very gently arcuate forward; depressions and elevations formed as a result of intersection of the **A** and **SAr** striation create a foveate pattern. **Ar** is arcuate forward, weakly and moderately convex, 0.12–0.17 times as long as **G**; $\mathbf{a_1Ar} : \mathbf{a_1A}$ = 0.6–0.88. **Bcl** is subrectangular, flattened, very weakly inclined inward and backward, its width is 0.19–0.28 of the **G** width in the middle. The palpebral furrows (sulci palpebrales, **SPal**) are weakly arcuate outward, much narrower and shallower than **SD**. **Pal** are weakly curved, weakly convex, subhorizontal, oriented slightly obliquely with regard to the axis; their anterior ends are situated a little closer to **SD** than their posterior ends; $\mathbf{a_1(c)Pal}$ is 0.43–0.54 times as long as **G**. The palpebral ridges are distinct, moderately convex, orientated obliquely toward the axis at an angle of approximately 50–60°, approaching **G** at one-sixth of the length of **G** from its anterior margin. The posterior parts of the fixigenae (**Fix**) are flattened, narrowly wedge-shaped, perpendicular to the axis. The posterior border

Plate 12

1

1a

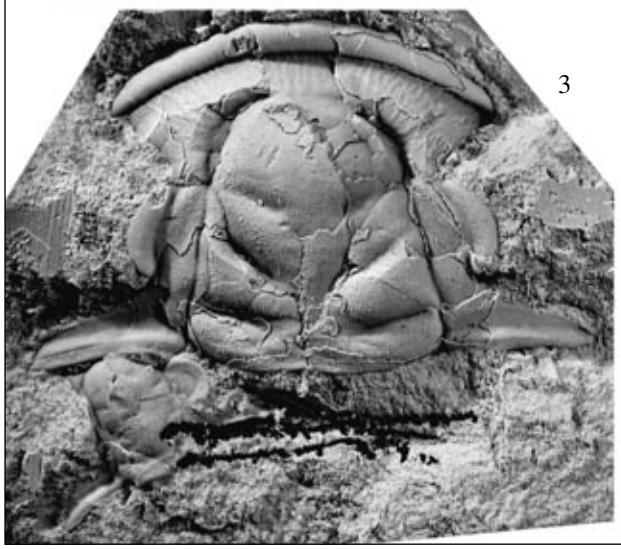

3

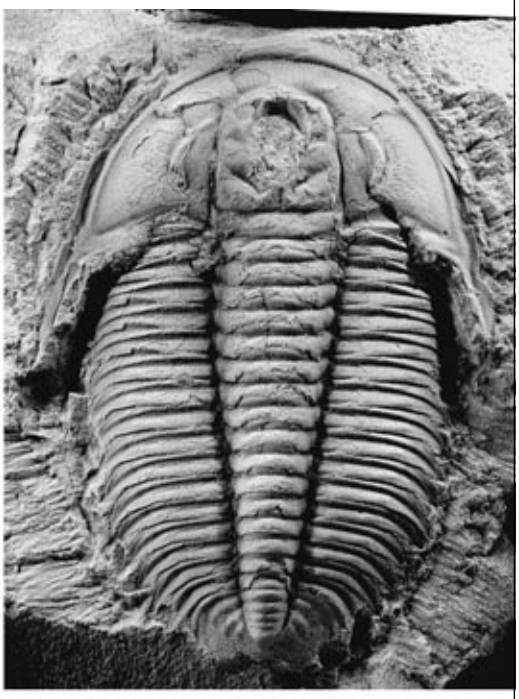

2

4

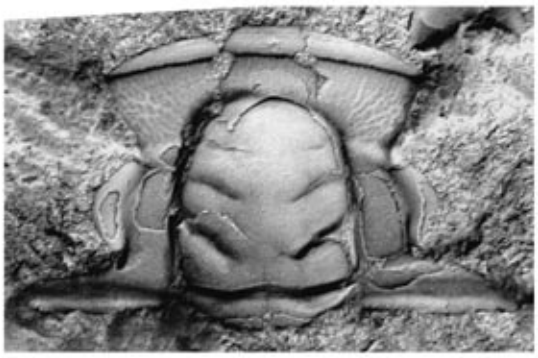

5

6

furrows are broad and deep, as deep as, and broader than **SD**, perpendicular to the axis, broadening and becoming shallower outwards. The posterior borders are weakly convex, perpendicular to the axis, of slightly variable width, weakly curved in the vertical plane, their width (transverse) is 0.65–0.98 the width of the **G** base. The anterior branches of the facial sutures are sharply divergent, straight, abruptly turning toward the axis after crossing **SAr**; the posterior branches of the facial sutures are very sharply divergent, almost transverse. The surface of **Cr** is generally finely punctate-granulated; there is striation with anastomoses on **A**, with striae being oriented subnormally to **SAr**.

The librigenae are irregularly trapezoidal, weakly convex and weakly inclined toward the sides. The lateral border furrows are very gently curved outward, narrower and shallower than **SD**; near the genal corners, they are fused with the posterior border furrows, which are broader and shallower than **SD**, at acute angles with narrow rounded connections. The posterior borders are flat, inclined abaxially, their length (longitudinal) is equal to the width (transverse) of the lateral border, which is flat, ribbonlike and weakly curved outward. Joining near the genal corners, the posterior and lateral borders form bases of long genal spines. Depressions orientated parallel to the genal spines are developed on the surface of the posterior borders near the points of junction. The genal spines are directed backward and slightly abaxially, gently narrowing and reaching, at least, the sixth segment of **T**. The genal limbs are weakly convex, with their anterior parts being narrower than the posterior ones. The surface of the librigenae is punctately granulated, the genal limbs are covered with anastomosing striation that is oriented almost perpendicular to the sides of **C**.

The **T** is cup-shaped, weakly convex, consisting of 16 segments, with its maximum width at the sixth segment; the ratio of its length to maximum width is 0.92. The axis of the **T** is narrowly wedge-shaped, widest near the anterior margin, gradually and evenly narrowing backwards to the eighth segment, beyond which it narrows slightly more abruptly; the axis is moderately convex, the ratio of the maximum width to the minimum width of the axis is 2.6; the axial furrow is almost straight, weakly converging backward, narrower and shallower than **SD**. The pleural fields are subrectangular, weakly convex, widest at the level of the sixth segment, their maximum width is 0.34 of the maximum width of **T**. The width (transverse) of segments increases very gradually from the anterior margin of the **T** to the sixth segment, then, gradually and evenly decreases backwards. Similarly, all other dimensions of the segments decrease backwards. The pleurae are parallel-sided for two-thirds of their length, and then gradually narrow toward their sides, bending backward and slightly downward, forming acuminate apices. In the transverse plane, the pleurae are weakly arcuate upward, their vertical curvature scarcely changes where they bend horizontally. Broad and moderately deep pleural furrows, which are orientated in general slightly obliquely with regard to the pleural margins, are traceable in the axial parts of the pleurae. Distinct convex ridges, which become abruptly thin and smooth in places where the pleurae are curved, extend along each side of the pleural furrows. The thinned regions of the ridges form dashed fulcral lines, weakly curved outward, which are also traceable on **Pyg**. The surface of the **T** is punctate granulated.

Pyg is transversely oval-shaped (excluding spines), weakly convex; $\mathbf{a_1Pyg} : \mathbf{b_{mx}Pyg} = 0.5–0.56$. The axis is moderately convex, conical, narrowing backward, 0.79–0.86 times as long as **Pyg**, the maximum width of the axis is one-third of the maximum width of **Pyg**. The axial furrows are narrow and relatively shallow, straight, converging backward. The first inter-ring furrow is deeper than the axial furrows, as broad as the latter near the axis, becoming shallower and narrower abaxially. The second furrow is narrower and shallower than the first, also becoming shallower and narrower along the axis. The third furrow is narrower and shallower than the second. The fourth furrow is barely visible, very narrow and shallow. The axis consists of four rings. The convexity, longitudinal and transverse dimensions of the axial rings decrease backward; the length (longitudinal) of the first ring is 0.18–0.21 of the axial length, the second ring is 0.15–0.19 times as long as the axis, the third ring is 0.13–0.15 times as long as the axis, and the fourth ring is 0.08–0.11 times as long as the axis. The terminal axial rings are moderately convex, with rounded angular posterior margins; the length (longitudinal) of the terminal ring is 0.28–0.34 of the axial length. The pleural fields are subtriangular, flattened, slightly inclined toward the sides; their maximum width is 0.21 of the maximum width of **Pyg**. Three to four pairs of pleurae, which are gently arcuate toward the anterolateral corners of **Pyg**, are recognizable. Transverse and longitudinal dimensions of pleu-

Explanation of Plate 12

Figs. 1–6. *Rybniites* (*Rybniites*) *spiculatus* Pack sp. nov.: (1) holotype CSGM, no. 749/23, **D** with complete exoskeleton, outcrop Ch-8-I-2, $\mathbf{a_1}$ of **D** = 42.8 mm, ×2.3; (1a) **Pyg** and fragment of **T**, detail of Fig. 1, $\mathbf{a_1}$ of **Pyg** = 5.9 mm, ×3.6; (2) paratype CSGM, no. 749/24, **D** with complete exoskeleton, outcrop Ch-8-I-2, $\mathbf{a_1}$ of **D** = 31.7 mm, ×2.6; (3) specimen CSGM, no. 749/25, distorted **Cr** with partially preserved exoskeleton, outcrop Ch-8-I-2, $\mathbf{a_1}$ of **Cr** = 15.7 mm, ×3, **Cr** of *Proceratopyge* also here; (4) specimen CSGM, no. 749/26, incomplete **Cr** with almost complete exoskeleton, outcrop Ch-8-I-2, $\mathbf{a_1}$ of **Cr** = 5.35 mm, ×8; (5) specimen CSGM, no. 749/27, **Cr** with partially preserved exoskeleton, outcrop Ch-8-I-2, $\mathbf{a_1}$ of **Cr** = 5.0 mm, ×7.6; (6) specimen CSGM, no. 749/28, incomplete **Cr** with partially preserved exoskeleton, outcrop Ch-8-I-2, $\mathbf{a_1}$ of **Cr** = 3.2 mm, ×10.

All specimens from the *Agnostotes* (*Pseudoglyptagnostus*) *clavatus–Irvingella perfecta* Zone.

rae decrease backward. Three pairs of curved, ridgelike, moderately convex ribs are developed at the margins of the pleurae; the length of the ribs decreases sharply backward; the interpleural furrows are recognizable with difficulty in the axial parts of the ribs. The border is weakly convex and narrow near the anterolateral corners of **Pyg**, flattens toward the posterolateral corners, forming along the axis two broadly triangular areas with their apices directed backward. Symmetrically narrowing, these areas transform into peaklike marginal spines, which are directed backward and barely visibly outward. The border is separated from the pleural fields by an interrupted border furrow, which is shaped as broad and shallow depressions within the pleurae and interrupted over the ribs; simultaneously, the border is separated from the pleural fields by smooth bends of the surface. These boundaries are natural extensions of the thoracic fulcral lines into **Pyg**. The surface of **Pyg** is punctately granulated.

Dimensions in mm and ratios:

Parameters	Specimen CSGM, no.				
	749/28	749/26	749/25	749/24	749/23
$\mathbf{a_1}$ of **D**	–	–	–	31.7	42.8
$\mathbf{a_1}$ of **C**	–	–	–	10.6	14.2
$\mathbf{a_1}$ of **T**	–	–	–	17.7	23.0
$\mathbf{a_1}$ of **Pyg**	–	–	–	3.9	5.8
$\mathbf{b_{mx}}$ of **D**	–	–	–	20.7	–
$\mathbf{b_{mx}}$ of **T**	–	–	–	19.2	26.3
$\mathbf{b_{mx}}$ of **Pyg**	–	–	–	7.5	10.4
$\mathbf{b_{mx}}$ of axis on **T**	–	–	–	6.8	9.3
$\mathbf{b_{min}}$ of axis on **T**	–	–	–	3.0	4.0
$\mathbf{a_1}$ of **Cr**	3.2	5.35	15.7	10.4	14.2
$\mathbf{a_1}$ of **Cor**	0.75	1.2	3.7	2.5	3.0
$\mathbf{a_1}$ of **Ar**	0.3	0.45	1.7	1.0	1.4
$\mathbf{a_1}$ of **A**	0.45	0.75	2.0	1.5	1.6
$\mathbf{a_1}$ of **G**	2.0	3.45	10.0	6.5	9.7
$\mathbf{a_1}$ of **O**	0.45	0.7	2.0	1.4	1.5
$\mathbf{b_1}$ of **Cr**	3.2	5.4	17.0	12.5	16.5
$\mathbf{b_3}$ of **Cr**	3.6	6.1	16.3	10.9	14.2
$\mathbf{b_5}$ of **Cr**	5.8	9.2	25.4	–	23.0
$\mathbf{b_3}$ of **G**	1.85	3.1	9.7	6.3	8.0
$\mathbf{b_5}$ of **G**	1.85	3.3	10.5	6.4	8.5
b of **Bcl**	0.5	0.8	1.9	1.4	1.7
b of posterior border	1.8	2.9	6.7	–	6.8
c of **Pal**	1.0	1.8	4.4	2.8	4.2
$\mathbf{a_1}$ of axis	–	–	–	3.1	5.0
$\mathbf{b_{mx}}$ of axis	–	–	–	2.5	3.9
$\mathbf{a_1}$ of M1 ring	–	–	–	0.65	0.9
$\mathbf{a_1}$ of M2 ring	–	–	–	0.6	0.75
$\mathbf{a_1}$ of M3 ring	–	–	–	0.45	0.65
$\mathbf{a_1}$ of M4 ring	–	–	–	0.4	0.5
$\mathbf{a_1}$ of **C** : $\mathbf{a_1}$ of **D**	–	–	–	0.33	0.33
$\mathbf{a_1}$ of **T** : $\mathbf{a_1}$ of **D**	–	–	–	0.55	0.53
$\mathbf{a_1}$ of **Pyg** : $\mathbf{a_1}$ of **D**	–	–	–	0.12	0.13
$\mathbf{a_1}$ of **T** : $\mathbf{b_{mx}}$ of **T**	–	–	–	0.92	0.87
$\mathbf{b_{mx}}$ of axis on **T** : $\mathbf{b_{mx}}$ of **T**	–	–	–	0.35	0.35
$\mathbf{b_{mx}}$ of axis on **T** : $\mathbf{b_{min}}$ of axis on **T**	–	–	–	2.27	2.33
$\mathbf{a_1}$ of **Cr** : $\mathbf{b_3}$ of **Cr**	0.89	0.88	0.96	0.95	1.0
$\mathbf{a_1}$ of **G** : $\mathbf{a_1}$ of **Cr**	0.63	0.64	0.64	0.64	0.68
$\mathbf{a_1}$ of **Cor** : $\mathbf{a_1}$ of **Cr**	0.23	0.22	0.24	0.24	0.21
$\mathbf{a_1}$ of **O** : $\mathbf{a_1}$ of **Cr**	0.12	0.14	0.13	0.13	0.11
$\mathbf{a_1}$ of **Ar** : $\mathbf{a_1}$ of **Cor**	0.67	0.6	0.65	0.67	0.88
$\mathbf{a_1}$ of **G** : $\mathbf{b_3}$ of **G**	1.08	1.11	1.03	1.03	1.21
b of **Bcl** : $\mathbf{b_3}$ of **G**	0.27	0.25	0.19	0.22	0.21
b of posterior border : $\mathbf{b_5}$ of **G**	0.98	0.91	0.65	–	0.85
c of **Pal** : $\mathbf{a_1}$ of **G**	0.5	0.52	0.44	0.43	0.43
$\mathbf{a_1}$ of **Pyg** : $\mathbf{b_{mx}}$ of **Pyg**	–	–	–	0.52	0.56
$\mathbf{a_1}$ of axis : $\mathbf{a_1}$ of **Pyg**	–	–	–	0.79	0.86
$\mathbf{a_1}$ of axis : $\mathbf{b_{mx}}$ of axis	–	–	–	1.24	1.25
$\mathbf{a_1}$ of M1 ring : $\mathbf{a_1}$ of axis	–	–	–	0.19	0.18
$\mathbf{a_1}$ of M2 ring : $\mathbf{a_1}$ of axis	–	–	–	0.15	0.15
$\mathbf{a_1}$ of M3 ring : $\mathbf{a_1}$ of axis	–	–	–	0.13	0.13
$\mathbf{a_1}$ of M4 ring : $\mathbf{a_1}$ of axis	–	–	–	0.10	0.08

Variability. Ontogenetic variability is expressed in increasing angles between the anterior branches of the facial sutures along with the growth of **Cr** at early holaspid stages of development. Additionally, the ratio of the length of **G** to the width of its base changes with growth from 1.08 to 0.99 (**G** becomes subquadrate in mature forms), the ratio of the length of **Pal** to the length of **G** decreases from 0.5 for small (up to 5 mm long) to 0.43 for large (over 10 mm) **G**. Individual variability includes variation of the ratios of the length (longitudinal) of **Ar** to the length (longitudinal) of **A** from 0.6 to 0.88, and of the width of **Bcl** to the width of **G** in the middle from 0.19 to 0.28.

Comparison. For comparison with the species *Rybniites* (*Rybniites*) *corniformis* sp. nov., see the description of the latter.

The new species differs from *Rybniites* (*Rybniites*) *borealis* (Lermontova, 1940) in having narrower **Bcl** that constitute less than 0.25 of the width of **G** in the middle (in *R.* (*R.*) borealis, the width (transverse) of **Bcl** is approximately 0.35 of the width of **G** in the middle), relatively shorter (longitudinal) **Ar**, smaller marginal spines of **Pyg**, and in a less distinct border furrow on the pygidium.

It differs from *?Rybniites* (*Rybniites*) *ludvigsensis* (Pratt, 1992) in having a shorter **G**, in a smaller length (longitudinal) of **Ar**, and in the presence of a node on **O**.

Distribution. Upper Cambrian, **A**gnostotes (*Pseudoglyptagnostus*) *clavatus–Irvingella perfecta* Zone.

Locality and Material. Ch-8-I-2: 2 **D** (well-preserved) and over 10 **Cr** (well and satisfactorily preserved).

***Rybniites* (*Rybniites*) *corniformis* Pack, sp. nov.**

Plate 13, figs. 1–4 and 5?

Etymology. From the Latin *corniformis* (hornlike), after the shape of the marginal spines on **Pyg**.

Holotype. CSGM, no. 749/29, **D**; northwestern Siberian Platform, Chopko River, Ch-17-I-2; Upper Cambrian, upper part of the **A**gnostotes (*Pseudoglyptagnostus*) *clavatus–Irvingella perfecta* Zone, Chopko Formation (Pl. 13, fig. 1).

Diagnosis. Representative of *Rybniites* (*Rybniites*) with basally broad hornlike marginal **Pyg** spines directed backward and slightly inward, with convex **Ar**, which is longer (longitudinally) than **A**, with elongated occipital node and supplementary transverse glabellar division.

Description. The **D** is elongated elliptical, weakly convex, flattened, 30.9 mm long; $\mathbf{a_1}$ of **C** : $\mathbf{a_1}$ of **D** = 0.31, $\mathbf{a_1}$ of T : $\mathbf{a_1}$ of **D** = 0.56, $\mathbf{a_1}$ of **Pyg** : $\mathbf{a_1}$ of **D** = 0.13. **Cr** are medium-sized and large (15.4 to 20.0 mm long), subtrapezoid, weakly convex, the ratio of the length of **Cr** to its width near the base is 0.85. **G** is moderately convex, subrectangular, with very smoothly rounded anterior end, 0.61–0.63 times as long as **Cr**, $\mathbf{a_1}$ of **G** : $\mathbf{b_3}$ of **G** = 1.04–1.08. **SD** are moderately broad and moderately deep, straight, very weakly converging forward, becoming much shallower near the anterolateral corners of **G** due to crossing the palpebral ridges, then immediately turn gently toward the axis and join **SPg**. Small fossulae are developed at the joint points; they are bent and slightly broader and deeper than **SD** that outline the anterolateral corners of **G**. **SPg** is weakly curved forward, narrower and shallower than **SD**, becoming even more shallower near the axis and becoming poorly distinguishable. **G** has three pairs of posteriorly oblique **SG**. $\mathbf{S_1G}$ originates from **SD** as two narrow and shallow branches, at 0.25 and 0.37 of the length from its posterior margin, respectively. Both branches are directed obliquely to the axis and merge at 0.12 of the **G** base width from **SD**, outlining small irregular rounded supplementary lobes $L^1$1; after fusion of $\mathbf{S_1G}$, they become very deep and broad (deeper and broader than **SD**), being directed obliquely inward and backward; their inner ends are situated at 0.12 of the length of **G** from its posterior margin and at 0.37 of the width of **G** from **SD**. Two pairs of muscle scars are observable in furrows $\mathbf{S_1G}$: one pair of large irregularly rounded scars is situated at the point where two branches of $\mathbf{S_1G}$ come into contact, the second pair is near their ends. On each side of the axis between $\mathbf{S_1G}$ and the posterior margin of **G**, there are two barely visible small supplementary furrows, which start at 0.07 and 0.13 of the length of **G** from its posterior margin and are perpendicular to the axis. The posterior furrows are shorter and traceable for 0.1 of the width of **G** base from **SD** on each side; the anterior furrows extend for 0.2 of the width of the **G** base from **SD**. Furrows $\mathbf{S_2G}$ originate at a distance from **SD**, at 0.52 of the length of **G** from its posterior margin, broader and deeper than **SD**, but narrower and shallower than $\mathbf{S_1G}$, stretching obliquely toward the axis and backward; their inner ends are situated at 0.45 of the length of **G** from its posterior margin and at 0.37 of the width of the **G** base from the axial furrows. In $\mathbf{S_2G}$, there are three pairs of muscle scars arranged in a row along the entire length of this furrow. Furrows $\mathbf{S_3G}$ are poorly visible, originate at a noticeable distance from **SD** at 0.75 of the length of **G** from its posterior margin, directed inward and slightly backward, very weakly curved forward; their inner ends are situated at 0.72 of the length of **G** from its posterior margin and at 0.3 of the width of **G** base from **SD**. **SO** is weakly sinuous; it is deep and broad near **SD**, broader and deeper than **SD**, weakly curved forward; a weakly anteriorly curved part of **SO** is observable near the axis, where it becomes broader and shallower then **SD**. Two pairs of muscle scars are visible in lateral parts of **SO** on each side. **O** is parallel-sided, with a weakly sinuous anterior margin and a weakly concave posterior margin, 0.18–0.21 times as long as **G**, with a small elongated occipital node on the axis. **Cor** is archlike, weakly convex, inclined forward from **G**, subdivided into **A** and **Ar**, the length (longitudinal) of **Cor** is 0.4–0.5 of the length of **G** and 0.26–0.27 of the length of **Cr**. **SAr** is very clear, arcuate forward, narrower and deeper than **SD**; depressions and elevations formed as a result of intersection of the **A** and **SAr** striation create a foveate pattern. **A** is weakly convex, flattened, inclined forward from **G**, its length (longitudinal) is 0.17–0.26 of the length of **G**. **Ar** is convex, gently arcuate forward, its length (longitudinal) is 1.02–1.54 of the length (longitudinal) of **A**, its posterior part is steeply inclined backward, its anterior part is gently inclined forward. **Bcl** are narrow, flattened, subhorizontal, their width (transverse) is 0.26 of the width of **G** in the middle. **SPal** are narrower and shallower than **SD**, curved outward. **Pal** are weakly convex, curved, orientated obliquely toward the axis, 0.56 times as long as **G**, their anterior ends are situated slightly closer to **SD** than posterior ends. The palpebral ridges are unclear, probably due to poor preservation, and orientated obliquely forward and inward. The posterior parts of the **Fix** are very narrowly wedge-shaped and transverse. The posterior border furrows are broader and deeper than **SD**, perpendicular to the axis. The posterior borders are convex, ridgelike, their width (transverse) is 0.6 of the width of **G** base and almost invariable. The anterior branches of the facial sutures are straight, sharply divergent; the posterior branches are very sharply divergent, transverse. The surface of the cranidium is punctate granulated, that of **A** is covered with anastomosing striation orientated subnormally to **SAr**. **Ar** is covered with thin, interlacing, wavy, subparallel filiform ridges, which are parallel to the anterior margin of **Cr**.

The librigenae are not preserved.

The **T** is cup-shaped, consists of 16 segments, being widest at the sixth segment, its length is equal to its maximum width. The axis of the **T** is weakly convex,

Plate 13

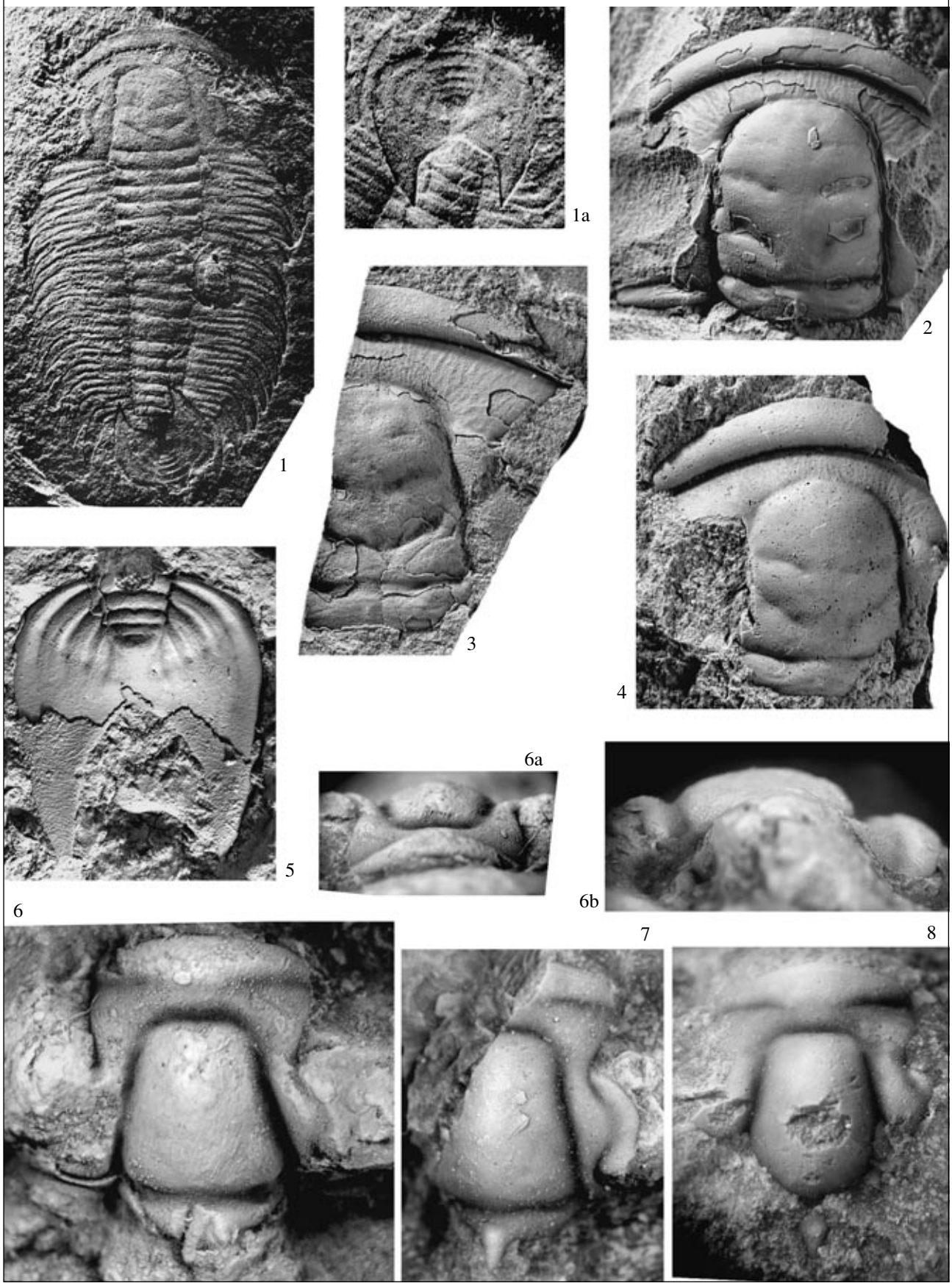

gradually narrowing backward, its maximum width is 0.37 of the maximum width of the **T**, the ratio of the maximum and minimum widths of the axis is 2.14. The axial furrows are almost straight, weakly converging backward, narrower and shallower than **SD**. The width of the **T** very weakly increases from the anterior margin to the sixth segment, and then gradually decreases toward the posterior margin. On the contrary, the length (longitudinal) of the segments is almost invariable. The pleurae are parallel-sided in areas adjoining the axis, perpendicular to the axis, bending backward and slightly downward in the form of acuminate spines near the **T** sides. The bending points are emphasized by changes in the relief of crests stretching along the pleurae, joining into interrupted fulcral lines, which gently curve to the sides. The moderately broad and deep pleural furrows orientated slightly obliquely backward with regard to the pleural margins extend along the pleurae.

Pyg is relatively small, with a conical narrowing backward axis that consists of four rings and the terminal piece . The pleural fields are weakly convex, subtriangular, with 3 or 4 pairs of pleurae and ribs, separated from the border by an interrupted border furrow, emphasized by bending of the surface. On each side of the axis behind the border furrow, there are flat triangular areas of the broadened border furrow that serve as the bases of hornlike marginal spines directed backward and toward the axis.

Dimensions in mm and ratios:

Parameters	Specimen CSGM, no.			
	749/29	749/31	749/32	749/30
$\mathbf{a_1}$ of **D**	30.9	–	–	–
$\mathbf{a_1}$ of **C**	9.6	–	–	–
$\mathbf{a_1}$ of **T**	17.3	–	–	–
$\mathbf{a_1}$ of **Pyg** (without spines)	4.0	–	–	–
$\mathbf{b_{mx}}$ of **T**	17.3	–	–	–
$\mathbf{b_{mx}}$ of **Pyg**	6.5	–	–	–
$\mathbf{b_{mx}}$ of axis on **T**	6.4	–	–	–
$\mathbf{b_{min}}$ of axis on **T**	3.0	–	–	–
$\mathbf{a_1}$ of **Cr**	9.6	20.0	17.5	15.3
$\mathbf{a_1}$ of **Cor**	2.5	6.25	4.67	3.91
$\mathbf{a_1}$ of **G**	5.9	12.5	10.67	9.75
$\mathbf{a_1}$ of **O**	1.2	2.5	2.33	1.67
$\mathbf{a_1}$ of **Ar**	1.5	2.92	2.83	2.08
$\mathbf{a_1}$ of **A**	1.3	3.33	1.83	1.83
$\mathbf{b_1}$ of **Cr**	–	26	19.67	–
$\mathbf{b_3}$ of **Cr**	–	–	–	–
$\mathbf{b_5}$ of **Cr**	11.3	–	–	–
$\mathbf{b_3}$ of **G**	6.2	12.0	10.0	9.0
$\mathbf{b_5}$ of **G**	–	12.67	10.0	9.0
b of **Bcl**	1.6	–	–	–
b of posterior border	3.9	–	–	–
c of **Pal**	3.3	–	–	–
$\mathbf{a_1}$ of axis	2.7	–	–	–
$\mathbf{b_{mx}}$ of axis	2.5	–	–	–
$\mathbf{b_{mx}}$ of pleural fields	–	–	–	–
$\mathbf{a_1}$ of **D** : $\mathbf{b_{mx}}$ of **D**	–	–	–	–
$\mathbf{a_1}$ of **C** : $\mathbf{a_1}$ of **D**	0.31	–	–	–
$\mathbf{a_1}$ of **T** : $\mathbf{a_1}$ of **D**	0.56	–	–	–
$\mathbf{a_1}$ of **Pyg** : $\mathbf{a_1}$ of **D**	0.13	–	–	–
$\mathbf{a_1}$ of **T** : $\mathbf{b_{mx}}$ of **T**	1.0	–	–	–
$\mathbf{b_{mx}}$ of axis on **T** : $\mathbf{b_{mx}}$ of **T**	0.37	–	–	–
$\mathbf{b_{mx}}$ of axis on **T** : $\mathbf{b_{min}}$ of axis on **T**	2.14	–	–	–
$\mathbf{a_1}$ of **Cr** : $\mathbf{b_5}$ of **Cr**	0.85	–	–	–
$\mathbf{a_1}$ of **G** : $\mathbf{a_1}$ of **Cr**	0.62	0.63	0.61	0.63
$\mathbf{a_1}$ of **Cor** : $\mathbf{a_1}$ of **Cr**	0.26	0.31	0.27	0.26
$\mathbf{a_1}$ of **Cor** : $\mathbf{a_1}$ of **G**	0.46	0.5	0.44	0.4
$\mathbf{a_1}$ of **Ar** : $\mathbf{a_1}$ of **A**	1.12	1.02	1.54	1.13
$\mathbf{a_1}$ of **G** : $\mathbf{b_3}$ of **G**	1.05	0.99	1.07	1.08
b of **Bcl** : $\mathbf{b_3}$ of **G**	0.26	–	–	–
c of **Pal** : $\mathbf{a_1}$ of **G**	0.56	–	–	–
b of posterior border : $\mathbf{b_5}$ of **G**	0.6	–	–	–
$\mathbf{a_1}$ of **Pyg** : $\mathbf{b_{mx}}$ of **Pyg**	0.6	–	–	–
$\mathbf{a_1}$ of axis : $\mathbf{a_1}$ of **Pyg**	0.66	–	–	–
$\mathbf{a_1}$ of axis : $\mathbf{b_{mx}}$ of axis	1.1	–	–	–

Explanation of Plate 13

Figs. 1–4, 5? *Rybniites* (*Rybniites*) *corniformis* Pack sp. nov.: (1) holotype CSGM, no. 749/29, **Cr**, **T,** and counterpart of **Pyg** without exoskeleton, outcrop Ch-17-I-2, $\mathbf{a_1}$ of (**Cr+T**) = 27 mm, ×2.6; (1a) detail of Fig. 1, counterpart of **Pyg**, $\mathbf{a_1}$ of **Pyg** = 3.9 mm, ×4.9; (2) specimen CSGM, no. 749/30, incomplete **Cr** with small remains of exoskeleton, outcrop Ch-21a, $\mathbf{a_1}$ of **Cr** = 15.3 mm, ×3.5; (3) specimen CSGM, no. 749/31, fragment of **Cr** with partially preserved exoskeleton, outcrop Ch-17-I-2, $\mathbf{a_1}$ of **Cr** = 20 mm, ×3; (4) specimen CSGM, no. 749/32, fragmentary **Cr** without exoskeleton, outcrop Ch-18-10, $\mathbf{a_1}$ of **Cr** = 17.5 mm, ×3; (5) specimen CSGM, no. 749/33, **Pyg** with small fragments of exoskeleton, outcrop Ch-19, total length of **Pyg** with spines = 21.7 mm, ×2.5.

Figs. 6–8. *Tchopkinella spinosa* Varlamov sp. nov.: (6) holotype CSGM, no. 749/41, fragmentary **Cr**, outcrop Ch-24-II-1, ×8; (6a) the same, frontal view; (6b) lateral view; (7) specimen CSGM, no. 749/43, fragment of **Cr**, outcrop Ch-26a-I-5, ×11.5; (8) specimen CSGM, no. 749/42, incomplete **Cr**, outcrop Ch-25-I-17, ×9.5.

Figs. 1, 3, and 5. Specimens from the upper part of the *Agnostotes* (*Pseudoglyptagnostus*) *clavatus–Irvingella perfecta* Zone. Figs. 2 and 4. Specimens from the *Norilagnostus quadratus–Irvingella cipita* Zone. Figs. 6–8. Specimens from the Zone *Irvingella norilica.*

Variability. The ratio of the length of **Ar** to the length of **A** ranges widely from 1.02 to 1.54 in available **Cr**.

Comparison. The new species differs from *Rybniites* (*Rybniites*) *spiculatus* sp. nov. in having the horn-shaped marginal spines on **Pyg**, which are directed backward and inward, in the longer (longitudinally) **Cor**, which is 0.26–0.27 times as long as **Cr** (**Cor** is 0.21–0.24 times as long as **Cr** in *R.* (*R.*) *spiculatus*), in the considerably more convex **Ar**, the length of which (longitudinal) is up to 1.5 times greater than the length of **A** (**Ar** is less convex and noticeably shorter than **A** in *R.* (*R.*) *spiculatus*), in the presence of a supplementary lobe L1, two pairs of additional furrows between furrows $\mathbf{S_1G}$ and the posterior margin of **G**, and an elongated occipital node.

R. (*R.*) *corniformis* sp. nov. differs from *Rybniites* (*Rybniites*) *borealis* (Lermontova, 1940) in having smaller marginal spines, narrower **Bcl**, longer **Ar**, in the presence of a supplementary lobe $L^1 1$, furrows between the posterior margin of **G** and $\mathbf{S_1G}$, and an elongated occipital node.

It differs from ?*Rybniites* (*Rybniites*) *ludvigsensis* (Pratt, 1992) in the presence of the occipital node, which is absent from *R.* (*R.*) *ludvigsensis*, supplementary furrows, and lobe $L^1 1$.

Remarks. **Pyg** depicted in Pl. 13, fig. 5 has been assigned to *R.* (*R.*) *corniformis* with some reservation, since, despite a similar overall structure, it has much larger marginal spines than **Pyg** of the holotype (Pl. 13, figs. 1, 1a).

Distribution. Upper Cambrian, upper part of the *Agnostotes* (*Pseudoglyptagnostus*) *clavatus–Irvingella perfecta* Zone and lower part of the *Norilagnostus quadratus–Irvingella cipita* Zone.

Locality and Material. **Ch-17-I-2**: 1 **D** (satisfactorily preserved) and 1 **Cr** (satisfactorily preserved); **Ch-18-10**: 1 incomplete **Cr** (satisfactorily preserved); **Ch-21a**: 1 incomplete **Cr** (satisfactorily preserved); and **?Ch-19**: 1 **Pyg**.

Subgenus *Rybniites* (*Pseudeugonocare*) Peng, 1992

Eugonocare (*Pseudeugonocare*) Peng, 1992: Peng, 1992, p. 60.

Type species. *Eugonocare* (*Pseudeugonocare*) *camptodromum* Peng, 1992, p. 62, figs. 31A–31F, text-fig. 34, China, northwestern Hunan, Cili–Taoyuan region, Wa'ergang section; Upper Cambrian, **A**gnostotes (*Pseudoglyptagnostus*) *clavatus–Irvingella angustilimbata* Zone, Bitiao Formation.

Diagnosis. **Pyg** axes consisting of 5–7 rings, pleural fields with 5 or 6 pairs of pleurae and ribs, **Cr** with broad **Bcl** constituting over 0.6 of **G** width in the middle, **Ar** always shorter (longitudinally) than and 0.6–0.7 times as long as **A**, **Cor** 0.3–0.35 times as long as **Cr**.

Species composition. *Rybniites* (*Pseudeugonocare*) *camptodromus* Peng, 1992. *Rybniites* (*Pseudeugonocare*) *hunanensis* (Zhou, 1977), China, northwestern Hunan, Cili–Taoyuan region; Upper Cambrian, *Innitagnostus inexpectans–Proceratopyge* (*Proceratopyge*) *protracta*, *Agnostotes* (*Pseudoglyptagnostus*) *clavatus–Irvingella angustilimbata* zones, Bitiao Formation, Wa'ergang and Shengjiawang sections.

Rybniites (*Pseudeugonocare*) *consimilis* (Ergaliev, 1980), Ergaliev, 1980, p. 123, pl. 12, figs. 16 and 17, Kazakhstan, Lesser Karatau, Kyr-Shabakty River; Upper Cambrian, Sakian, *Pseudagnostus "curtare"* Zone.

Rybniites (*Pseudeugonocare*) *bispinatus* (Kobayashi, 1935), Kobayashi, 1935, p. 101, pl. 7, figs. 1–7, South Korea; Upper Cambrian, Machari Formation.

Remarks. Peng (1992, p. 60) included *Crepicephalus borealis* Lermontova, 1940 in the subgenus *Eugonocare* (*Pseudeugonocare*). We transfer this species to the subgenus *Rybniites* (*Rybniites*) subgen. nov., since **Pyg** of *C. borealis* has a short axis with four rings and **Cr** has narrow **Bcl**, which are considerably narrower than those of the subgenus *Rybniites* (*Pseudeugonocare*) Peng.

Distribution. China, northwestern Hunan, Cili–Taoyuan region; Upper Cambrian, *Innitagnostus inexpectans–Proceratopyge* (*Proceratopyge*) *protracta* and *Agnostotes* (*Pseudoglyptagnostus*) *clavatus–Irvingella angustilimbata* zones; Kazakhstan, Lesser Karatau, Kyr-Shabakty River; Upper Cambrian, Sakian, *Pseudagnostus "curtare"* Zone; South Korea; Upper Cambrian, Machari Formation.

Genus *Tchopkina* Varlamov et Rosova, gen. nov.

Etymology. After the Chopko River.

Type species. *Tchopkina tchopkinica* Varlamov et Rosova, sp. nov., northwestern Siberian Platform, Norilsk District, Chopko River; Upper Cambrian, **A**gnostotes (*Pseudoglyptagnostus*) *clavatus–Irvingella perfecta, Norilagnostus quadratus–Irvingella cipita* and *Irvingella norilica* zones, Chopko Formation.

Diagnosis. Cranidium (**Cr**) medium-sized (7–12 mm), subquadrate ($\mathbf{a_1}$ of **Cr** approximately equal to $\mathbf{b_3}$ of **Cr**). Glabella (**G**) truncated conical, angularly rounded anteriorly, usually with poorly defined 2 or 3 pairs of glabellar furrows (**SG**, sulci glabellares) starting from axial furrow (**SD**, sulcus dorsalis). Median preglabellar furrow (**SPg**, sulcus preglabellaris) straight. **Cor** medium-sized (approximately 0.5 of $\mathbf{a_1}$ of **G**), clearly subdivided into equal frontal field (**A**, area) and anterior border (**Ar**, arculum). Anterior border furrow (**SAr**, sulcus arcularis) shallow and almost straight adaxially, deeper and turned forward and downward abaxially, depressed in form of oval-shaped foveae on boundary with **Cp**. **Cp** clearly separated in shape of small swelling, from which flat lateral areas of frontal field (**Tm**, tempus) sharply sloping diagonally downward. Anterior margin of **Cor** weakly arcuate. Palpebral area of fixigena (**Bcl**, buccula) not

broad (**bBcl** approximately 0.3 times as broad as $\mathbf{b_3G}$), sharply inclined to **G**; highest point of **Bcl** usually much higher (rarely slightly higher) than highest point of **G**. Occipital furrow (**SO**, sulcus occipitalis) weakly saddle-shaped. Occipital ring (**O**, occiput) small, bearing medium-sized node. Palpebral lobes (**Pal**, palpebra) medial, large (**a** of **Pal** equal to or more than 0.5 of $\mathbf{a_1}$ of **G**), parallel to longitudinal line of **Cr** and inclined to **G**. Posterior part of fixigena (**Fix**) relatively small, subtriangular, strongly extended abaxially. Posterior border furrow broadening near **O**, but shallower than **SD**, becoming broader and shallower toward sides. Posterior border of **Cr** weakly extended, broadening and flattening outward, constituting 0.7 of $\mathbf{b_5}$ of **G**. Anterior branches of facial sutures weakly diverging, posterior branches sharply diverging. Surface of **Cr** punctated foveate or smooth.

Comparison. The new genus is most similar to *Amorphella* Rosova (Rosova, 1963, p. 14) from the stratotype of the Yuraki Horizon of the Upper Cambrian (Kulyumbe River), but differs in the much larger **Cor** ($\mathbf{a_1Cor}$ = 0.48, that is, 0.55–0.57 of $\mathbf{a_1G}$, whereas in *Amorphella*, $\mathbf{a_1Cor}$ = 0.33, that is, 0.27–0.40 of $\mathbf{a_1G}$); in the **SAr** shallow adaxially and very clear and wide abaxially (in **A**morphella, **SAr** is only slightly narrower and shallower adaxially than abaxially); in the highest point of **Bcl** located higher than the highest point of **G** (whereas it is vice versa in *Amorphella*).

The new genus differs from *Nganasanella* Rosova (Rosova, 1963, p. 9; 1964, p. 71) from the stratotype of the Kulyumbe Regional Stage of the Upper Cambrian (Kulyumbe River) in having a subquadrate **Cr** (**Cr** is elongated in *Nganasanella*); in the presence of a swelling on **Cp**; in high **Bcl**, where, unlike in *Nganasanella*, the highest point of **Bcl** is higher than the highest point of **G**; in **Pal** being longer (**aPal** is approximately 0.5 of $\mathbf{a_1G}$, whereas **aPal** is approximately 0.4 of $\mathbf{a_1G}$ in *Nganasanella*); in the straight **SPg** (arcuate in *Nganasanella*); and in the very shallow adaxially **SAr** (**SAr** is almost uniform along its entire length in *Nganasanella*).

Distribution. Upper Cambrian, **A**gnostotes (*Pseudoglyptagnostus*) *clavatus–Irvingella perfecta, Norilagnostus quadratus–Irvingella cipita* and *Irvingella norilica* zones.

***Tchopkina tchopkinica* Varlamov et Rosova, sp. nov.**

Plate 14, figs.1–5

Etymology. After the Chopko River.

Holotype. CSGM, no. 749/35, **Cr**; northwestern Siberian Platform, Norilsk District, Chopko River, faunal site 123; Upper Cambrian, middle part of the *Agnostotes* (*Pseudoglyptagnostus*) *clavatus–Irvingella perfecta*, Zone, Chopko Formation (Pl. 14, fig. 1).

Diagnosis. **Cr** with relief; **Bcl** high, almost steep, highest point of **Bcl** is much higher than highest point of **G**; **Ar** elevated above **A**.

Description. **Cr** is medium-sized ($\mathbf{a_1Cr}$ = 7–12 mm), moderately convex, subquadrate ($\mathbf{a_1}$ of **Cr** is approximately equal to $\mathbf{b_3}$ of **Cr**), with relief, with prominent posterior parts of **Fix** and steep **Bcl**. The highest point of **Cr** is at the midlength of **Pal**.

G is truncated conical ($\mathbf{b_1G}$ = 0.48, that is, 0.50–0.57 of $\mathbf{b_5G}$), moderately convex, with weakly rounded anterolateral corners, keeled. The sagittal profile of **G** is moderately arcuate, being steeper anteriorly than posteriorly. The highest point of **G** is in its center or slightly shifted posteriorly. The transverse profile of **G** is regularly arcuate. **SD** are straight, narrow and deep, uniform along their entire length, smoothly run into a similarly deep and broad, straight **SPg**, angularly surrounding **G**. **SD** become considerably shallower opposite the anterolateral corners of **G**. There are 2 or 3 pairs of **SG**, which are shallow and unclear on the exoskeleton. $\mathbf{S_1G}$ are oblique, weakly S-shaped, shallower but broader than **SD**. $\mathbf{S_2G}$ are straight, obliquely orientated, as broad as, but shallower and shorter than, $\mathbf{S_1G}$. $\mathbf{S_3G}$ are subtransverse and barely visible. All **SG** start at **SD**. Laterally, **SO** is as broad as and as deep as **SD**; adaxially it is shallower and arcuate forward. **O** is broadened in the middle ($\mathbf{a_1O}$ is 0.25 of $\mathbf{a_1G}$) and narrows toward the sides. The highest point of **O** is a little lower than, or sometimes at the same level as the highest point of **G**. **O** has a medium-sized node, which is situated in the middle or slightly shifted backward.

Cor is medium-sized ($\mathbf{a_1Cor}$ = 0.32, that is, 0.30–0.33 of $\mathbf{a_1Cr}$, $\mathbf{a_1Cor}$ = 0.55, that is, 0.48–0.57 of $\mathbf{a_1G}$), distinctly subdivided into **Ar**, **Cp**, and **Tm**. **Cp** is weakly convex, inclined forward, the highest point of **Cp** is lower than the highest point of **Ar**. **Tm** are almost flat, sharply inclined from **Cp** to the anterolateral corners of **Cr**. **SAr** is weakly arcuate backward, almost straight in the middle, sometimes poorly noticeable. **SAr** are more distinct and deeper abaxially than adaxially, broad, diffused, but narrower and shallower than **SD**, depressed in the form of ovoid pits at the boundary with **Cp**. **Ar** is lens-shaped, convex, $\mathbf{a_1Ar}$ is approximately equal to $\mathbf{a_1A}$.

Bcl are not broad (**bBcl** = 0.35, that is, 0.33 of $\mathbf{b_3G}$), weakly convex, high, almost perpendicularly elevated over **G** and steeply lowering toward **Tm** and the posterior part of **Fix**. The highest point of **Bcl** is on the boundary with **SPal** and is higher than the highest point of **G**. The posterior part of **Fix** is relatively small, less than 0.3 of $\mathbf{a_1G}$, weakly convex, subtriangular, drawn abaxially and abruptly inclined from **Bcl** downward and toward the posterolateral corners of **Cr**. The posterior border furrow near **O** is broader but shallower than **SD**, broadening and shallowing toward the sides. The posterior border of **Cr** is weakly convex, medium-sized (approximately 0.7 of $\mathbf{b_5G}$), smaller than $\mathbf{a_1O}$ on the boundary with **O**, becoming larger and flatter toward the sides. **Pal** are medial, large (**aPal** is equal to or greater than 0.5 of $\mathbf{a_1G}$, **bPal** is 0.50 of **bBcl**), weakly convex, weakly arcuate, parallel to **Cr**. The highest

Plate 14

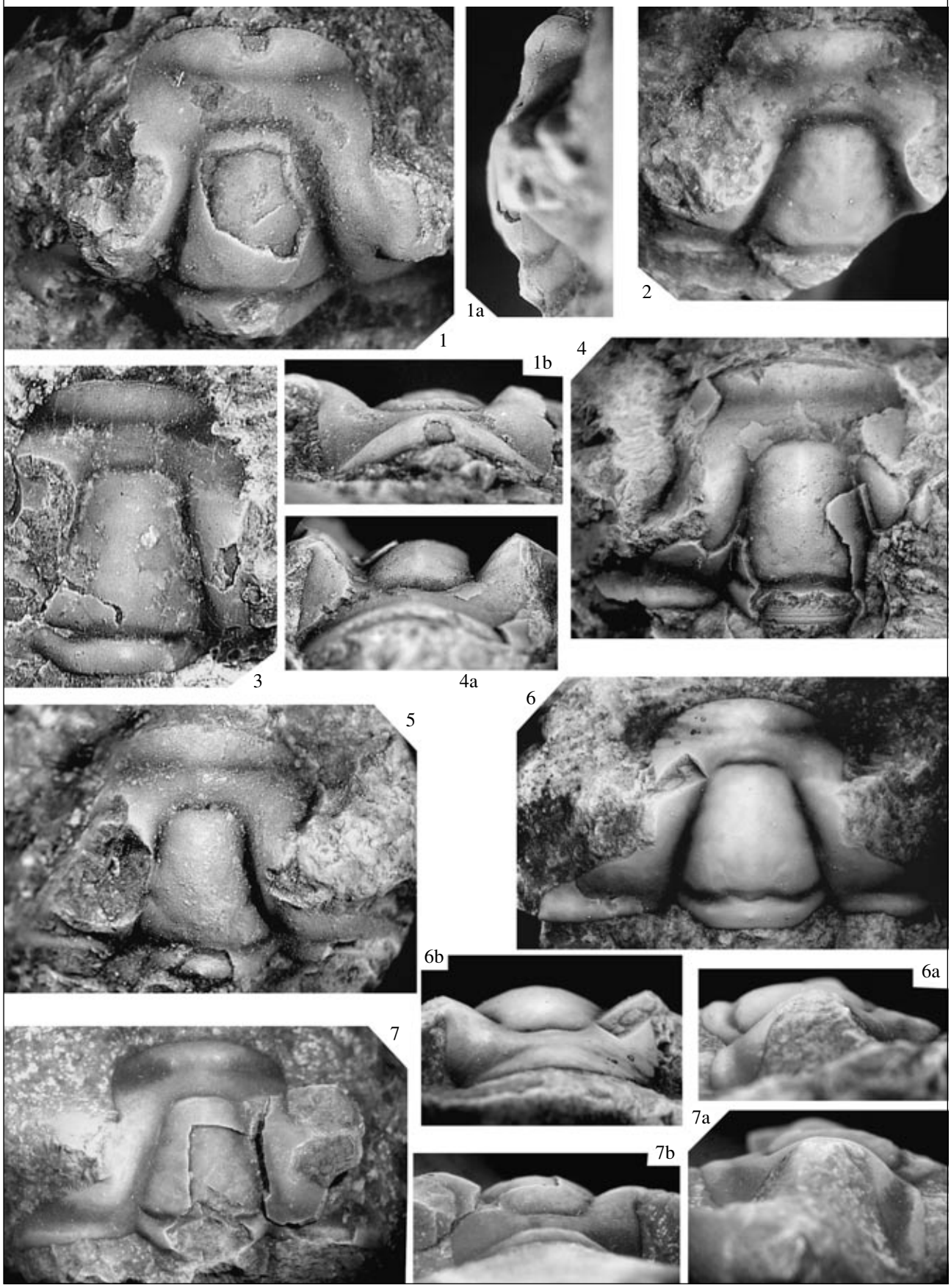

point of **Pal** is higher than the highest point of **G**, **SPal** are considerably shallower and narrower than **SD** (on exoskeleton). The palpebral ridges are barely visible, approach **G** at one-sixth of $\mathbf{a_1G}$ from the anterior margin of **G**.

The anterior branches of the facial sutures are weakly diverging up to **SAr**, then, arching to the longitudinal axis of **Cr**. The posterior branches are diagonally diverging. The surface of **Cr** is smooth or irregularly covered near the **Cr** axis with nodes of varying sizes.

Variability. **Cor** varies from medium-sized (a little smaller than 0.5 of $\mathbf{a_1G}$) to large (over 0.5 of $\mathbf{a_1G}$). The highest point of **Bcl** is usually much higher than the highest point of **G**, but in individual specimens it is slightly higher. The clearness of the keel and $\mathbf{S_3G}$ and the size of pitlike depressions on **SAr** of **Cr** are variable.

Comparison. See under the description of *Tchopkina plana* sp. nov.

Distribution. Upper Cambrian, **A**gnostotes (*Pseudoglyptagnostus*) *clavatus–Irvingella perfecta, Norilagnostus quadratus–Irvingella cipita* and *Irvingella norilica* zones.

Locality and Material. Ch-11-I-3: 2 **Cr** (well-preserved) and 3 **Cr** (satisfactorily preserved); Ch-22-II-1: 1 **Cr** (well-preserved); and Ch-24-II-1: 1 **Cr** (well-preserved).

***Tchopkina plana* Rosova et Makarova, sp. nov.**

Plate 14, figs. 6 and 7

Etymology. From the Latin *plana* (flat).

Holotype. CSGM, no. 749/40, **Cr**; northwestern Siberian Platform, Norilsk District, Chopko River, outcrop **Ch-10d**; Upper Cambrian, middle part of the **A**gnostotes (*Pseudoglyptagnostus*) *clavatus–Irvingella perfecta* Zone, Chopko Formation (Pl. 14, fig. 6).

Diagnosis. **Cr** flattened, without relief; **Bcl** not high, steeply inclined to **G**. Highest point of **Bcl** slightly higher than **G**; small ridge discernible on **Cp** near **SPg**; **Ar** slightly lower than **A**. $\mathbf{S_1G}$ long, branching.

Description. **Cr** is medium-sized ($\mathbf{a_1Cr}$ = 8–9 mm), subquadrate ($\mathbf{a_1Cr}$ is approximately equal to $\mathbf{b_3Cr}$), weakly convex, flattened. The anterior margin of **Cr** is weakly arcuate. **G** is truncated conical ($\mathbf{b_1G}$ = 0.47, that is, 0.43 of $\mathbf{b_5G}$). The sagittal profile of **G** is regularly gently arcuate, almost horizontal in the middle, smoothly lowering laterally to **SPg** and **SO**. The transverse profile is gently arcuate. There are two pairs of **SG**; they are very unclear, start from **SD** and are visible only in oblique illumination. $\mathbf{S_1G}$ are long, oblique, in the shape of very small notches, which are as broad as **SD**, bifurcate at 0.25 of $\mathbf{a_1G}$: the posterior branch closely approaches **SO**, the anterior branch closely approaches the midlength of **G**. $\mathbf{S_2G}$ are subtransverse, as broad as but shallower than $\mathbf{S_1G}$. **SG** are practically invisible on casts. **SD** are straight, medium-wide and deep, shallower on the boundary with **SPg**. **SPg** is straight, as broad as and as deep as **SD**.

SO is saddle-shaped, abaxially as broad as and as deep as **SD**, adaxially shallower and broader, with a small bend oriented backward. **O** is adaxially broadened ($\mathbf{a_1O}$ is 0.20 of $\mathbf{a_1G}$) and narrows toward the sides. The highest point of **O** is slightly lower than the highest point of **G**. The posterior margin of **O** is almost straight adaxially. There is a small node in the center of **O**.

Cor is medium-sized ($\mathbf{a_1Cor}$ = 0.48, that is, 0.45 of $\mathbf{a_1G}$), weakly convex, distinctly subdivided into equal **A** and **Ar**. In profile, **A** and **Ar** are similarly sloping downward, with a small bend of the surface at the level of **SPg**. The highest point of **A** is much lower than the highest point of **G** and slightly higher than the highest point of **Ar**. **SAr** is adaxially almost straight and considerably shallower and narrower than **SD**, abaxially with a small bend oriented forward and downward, broadening outward, and becoming deeper on the boundary with **Cp** and forming small oval-shaped foveae. **Cp** is in the shape of a small swelling, with a supplementary weak ridge in its posterior half.

Bcl are not broad ($\mathbf{bBcl}$ = 0.34, that is, 0.38 of $\mathbf{b_3G}$), weakly convex, steeply inclined to **G**. The highest point of **Bcl** is slightly higher than the highest point of **G**. The posterior part of **Fix** is small (0.3 of $\mathbf{a_1G}$), weakly convex, subtriangular, drawn abaxially and sharply inclined from **Bcl** downward and to the posterolateral corners of **Cr**. The posterior border furrow near **O** is broader but shallower than **SD**, broadening and shallowing toward the sides. The posterior marginal border of **Cr** is large (= 0.91, that is, 0.77 of $\mathbf{b_5G}$), weakly convex, smaller than $\mathbf{a_1O}$ on the boundary with **O**, enlarging toward the sides. **Pal** are medial, medium-sized ($\mathbf{aPal}$ = 0.44, that is, 0.45 of $\mathbf{a_1G}$), almost parallel to the longitudinal axis of **Cr**. The highest point of **Pal** is

Explanation of Plate 14

Figs. 1–5. *Tchopkina tchopkinica* Varlamov et Rosova sp. nov.: (1, 1a, 1b) holotype CSGM, no. 749/35, **Cr**, faunal site 123, ×10; (1a) lateral view; (1b) frontal view; (2) specimen CSGM, no. 749/38, **Cr**, faunal site 123, ×6; (3) specimen CSGM, no. 749/61, **Cr**, outcrop Ch-11-I-3, ×7; (4, 4a) specimen CSGM, no. 749/36, **Cr**, outcrop Ch-24-II-1, ×6; (4a) frontal view; (5) specimen CSGM, no. 749/37, **Cr**, outcrop Ch-22-II-1, ×7.

Figs. 6 and 7. *Tchopkina plana* Rosova et Makarova sp. nov.: (6, 6a, 6b) holotype CSGM, no. 749/40. **Cr**, outcrop Ch-10d, ×5; (6a) lateral view; (6b) frontal view; (7, 7a, 7b) specimen CSGM, no. 749/39, **Cr**, outcrop Ch-10d, ×4.5; (7a) lateral view; (7b) frontal view.

Figs. 1–3, 6, and 7. Specimens from the *Agnostotes* (*Pseudoglyptagnostus*) *clavatus–Irvingella perfecta* Zone. Fig. 4. Specimen from the *Irvingella norilica* Zone. Fig. 5. Specimen from the *Norilagnostus quadratus–Irvingella cipita* Zone.

higher than the highest point of **G**. The palpebral ridges are poorly traceable.

The anterior branches of the facial sutures are almost parallel to each other, the posterior branches diverge. The surface of **Cr** is smooth.

Comparison. The new species differs from *Tchopkina tchopkinica* Varlamov et Rosova, sp. nov. in having a flattened **Cr**, low **Bcl** with the highest point being slightly higher than the highest point of **G** (it is much higher in *T. tchopkinica*), in **Bcl** inclined to **G** at a smaller angle, in **Pal** being smaller (**aPal** is less than a half of $\mathbf{a_1G}$, whereas, in *T. tchopkinica*, **aPal** is equal to, or more than a half of $\mathbf{a_1G}$), in the presence of a supplementary ridge on **Cp** and in **SO** being saddle-shaped, whereas, in *T. tchopkinica*, it has an anterior curvature in the middle.

Distribution. Upper Cambrian, **A**gnostotes (*Pseudoglyptagnostus*) *clavatus–Irvingella perfecta* Zone.

Locality and Material. **Ch-10d**: 2 **Cr** (well-preserved).

Genus *Tchopkinella* Varlamov, gen. nov.

Etymology. After the Chopko River.

Type species. *Tchopkinella spinosa* Varlamov, sp. nov.; northwestern Siberian Platform, Norilsk District, Chopko River; Upper Cambrian, **A**gnostotes (*Pseudoglyptagnostus*) *clavatus–Irvingella perfecta, Norilagnostus quadratus–Irvingella cipita* and *Irvingella norilica* zones.

Diagnosis. **Cr** small or medium-sized ($\mathbf{a_1Cr}$ = 3–7 mm), moderately convex, subquadrate ($\mathbf{a_1Cr}$ approximately equal to $\mathbf{b_3Cr}$ without spine). **G** truncated conical, with two pairs of weak **SG** or smooth. **SD** deep, medium wide, straight, weakly converging anteriorly. **SPg** almost straight, as broad as and as deep as **SD**. **Cor** medium-sized ($\mathbf{a_1Cor}$ constituting 0.4–0.5 of $\mathbf{a_1G}$), subdivided into **A** and **Ar** ($\mathbf{a_1A}$ less than or equal to a half of $\mathbf{a_1Ar}$). **SAr** distinct, arcuate backward, which causes peculiar shape of **Ar** that hangs as peak over **A**. **Bcl** narrow, not high, abruptly inclined to **G**; highest point of **Bcl** equal to or lower than highest point of **G**. **SO** almost straight, slightly curving forward only abaxially. **O** attenuated into acute spine, which is longer than **O**. **Pal** medial, large (**aPal** more than or equal to 0.5 of $\mathbf{a_1G}$; **bPal** little less than **bBcl**). On casts, **SPal** very broad, just little less than **bPal**. Anterior branches of facial sutures diverging. **Cr** surface finely tuberculate or smooth.

Comparison. The new genus differs from the genus *Tchopkina* Varlamov et Rosova in the structure of **Bcl** with the highest point being lower than or at the same level as the highest point of **G** (in *Tchopkina*, the highest point of **Bcl** is much higher than the highest point of **G**) and in the smaller **A** ($\mathbf{a_1A}$ is less than, or equal to 0.5 of $\mathbf{a_1Ar}$, whereas $\mathbf{a_1A}$ is approximately equal to $\mathbf{a_1Ar}$ in *Tchopkina*).

Distribution. Upper Cambrian, *Agnostotes* (*Pseudoglyptagnostus*) *clavatus–Irvingella perfecta, Norilagnostus quadratus–Irvingella cipita* and *Irvingella norilica* zones.

Tchopkinella spinosa Varlamov, sp. nov.

Plate 13, figs. 6–8

Etymology. From the Latin *spina* (spine).

Holotype. CSGM, no. 749/41, **Cr**; northwestern Siberian Platform, Norilsk District, Chopko River, Ch-24-II-1; Upper Cambrian, lower third of the *Irvingella norilica* Zone, Chopko Formation (Pl. 13, fig. 6).

Diagnosis. This is the only species in this genus.

Description. **Cr** is medium-sized or large (7–11 mm), moderately convex, subquadrate ($\mathbf{a_1Cr}$ is approximately equal to $\mathbf{b_3Cr}$ without the spine). **G** is moderately convex, truncated conical ($\mathbf{b_1G}$ = 0.51, that is, 0.50–0.55 of $\mathbf{b_5G}$), with rounded anterolateral corners. The sagittal profile of **G** is regularly moderately arcuate, sometimes with the highest point of **G** shifted anteriorly. The transverse profile of **G** is regularly moderately arcuate. **G** usually has two pairs of **SG**, sometimes smoothed. $\mathbf{S_1G}$ are long, S-shaped, shallow and unclear; $\mathbf{S_2G}$ are oblique, straight, and shorter and less distinct than $\mathbf{S_1G}$. All **SG** originate immediately from **SD**. **SD** are deep, medium-wide, straight, sometimes with a small curvature in front of the **G** center toward the longitudinal axis of **Cr**. **SD** is continued by the equally broad and deep **SPg**, smoothly bordering the anterolateral corners of **G**. **SPg** is almost straight. **Cor** is medium-sized ($\mathbf{a_1Cor}$ is 0.41, that is, 0.42–0.48 of $\mathbf{a_1G}$), clearly subdivided into **A** and **Ar** ($\mathbf{a_1A}$ is less than, or equal to 0.5 of $\mathbf{a_1Ar}$). Laterally, **SAr** is shallower and narrower than **SD**, becoming even narrower and shallower adaxially, being sometimes barely noticeable. **SAr** is arcuate backward, which causes the peculiar shape of **Ar** that hangs as a peak over **A**. The highest point of **Ar** is higher than the highest point of **A**. **Cp** has a small swelling, from which the almost flat **Tm** are slightly inclined downward. **Bcl** are narrow (**bBcl** is 0.27, that is, 0.38 of $\mathbf{b_5G}$), not high, abruptly inclined to **G**; the highest point of **Bcl** is at the same level as, or lower than the highest point of **G**. Adaxially, **SO** is almost straight, as broad as and as deep as **SD**; abaxially, it is slightly narrower and shallower and slightly curved anteriorly. **O** is relatively small, adaxially broadened ($\mathbf{a_1O}$ is 0.19, that is, 0.18–0.23 of $\mathbf{a_1G}$ without the spine), narrows toward the sides, and has an acute spine oriented slightly upward from the posterior margin of **O**. The length of the spine is greater than the medial length of **O**. **Pal** are medial, large (**aPal** is equal to, or greater than 0.5 of $\mathbf{a_1G}$; **bPal** is slightly less than $\mathbf{b_3Bcl}$), arcuate, and parallel to the longitudinal axis of **Cr**. On casts, **SPal** are very broad, slightly narrower than **bPal**. The anterior branches of the facial sutures diverge. The surface of **Cr** is finely tuberculate or smooth.

Variability. The size of **Cor** and the angle of inclination of **Bcl** to **G** are variable.

Distribution. Upper Cambrian, Agnostotes (*Pseudoglyptagnostus*) *clavatus–Irvingella perfecta, Irvingella norilica* zones.

Locality and Material. Ch-11-I-3: 2 **Cr** (well-preserved); Ch-24-II-1: 1 **Cr** (well-preserved); Ch-25-I-17: 1 **Cr** (satisfactory preserved); and Ch-25a-I-5: 1 **Cr** (well-preserved).

Family Elviniidae Kobayashi, 1935

Genus *Irvingella* Ulrich et Resser, 1924

***Irvingella cipita* Varlamov et Rosova, sp. nov.**

Plate 15, figs. 1–5

Etymology. From the Latin *cipitis* (sphere-headed).

Holotype. CSGM, no. 749/67, **Cr**; northwestern Siberian Platform, Norilsk District, Chopko River, **Ch-15-I-5**; Upper Cambrian, bottom of the *Norilagnostus quadratus–Irvingella cipita* Zone, Chopko Formation (Pl. 15, figs. 1, 1a, 1b).

Diagnosis. **G** elongated, its anterior part hanging over **Cor**.

Description. **Cr** is medium-sized ($\mathbf{a_1G}$ is 8–9.5 mm), trapezoid. The anterior margin of **Cr** is arcuate downward.

G is strongly convex, elongated ($\mathbf{a_1G}$ is 1.54 of $\mathbf{b_3G}$), almost parallel-sided in its posterior three quarters, then it forms semi-ellipse, rounding the posterolateral corners of **G**. The sagittal profile of **G** is irregularly arcuate—the posterior section of the arch is slightly inclined backward and the anterior section, sharply turning, forms a semicircle. The highest point of **G** is situated at the level of 0.23 of $\mathbf{a_1G}$ from the anterior margin of **G**. The transverse profile of **G** is steeply arcuate, with the lateral sides of the arch weakly converging. **G** has 2 or 3 pairs of **SG**, which start at a distance from **SD**. $\mathbf{S_1G}$ is a distinct $\mathbf{S_1Tg}$, being narrower and deeper than **SD**. $\mathbf{S_1Tg}$ is broader and shallower adaxially than abaxially. The transverse lobe of **G** is narrowed adaxially (one-quarter of $\mathbf{a_1G}$) and slightly broadened to the sides. $\mathbf{S_2G}$ are shallow, narrow, short and subtransverse. $\mathbf{S_3G}$ are even shorter, shallower and narrower. **SD** are straight, broad, shallow, subparallel, starting to converge smoothly only opposite the highest point of **G** and becoming a slightly shallower and narrower **SPg**, rounding the anterolateral corners of **G**. **SO** is arcuate backward, narrower and deeper than **SD**, broader and shallower adaxially than abaxially. **O** is small, equal to the transverse lobe of the glabella, and almost equally broad along its entire extent. The highest point of **O** is considerably lower than the highest point of **G**. The posterior margin of **O** is weakly arcuate.

Cor is very small ($\mathbf{a_1Cor}$ is 0.05 of $\mathbf{a_1G}$), represented by **Ar** and **Tm** only (**Cp** is absent). **Ar** is ridgelike, uniform along its entire extent, weakly arcuate downward; in plane, it is weakly arcuate backward. The highest point of **Ar** is considerably lower than the highest point of **G**. **Tm** are very small, weakly convex, subhorizontal.

Bcl are medium-sized (**bBcl** is 0.5 of $\mathbf{b_3G}$), flattened, inclined outward from **SD**. The highest point of **Bcl** is much lower than the highest point of **G**. The posterior part of **Fix** is very small. Near **O**, the posterior border furrow is narrower and deeper than **SD**, and becomes broadener and deeper abaxially. The posterior border is narrow, ridgelike, approximately equal to the posterior part of **Fix**, slightly broadening abaxially. **SPal** is slightly narrower and deeper than **SD**. **Pal** are medial, large (**cPal** is approximately 0.86 of $\mathbf{a_1G}$), and curved. The posterior margin of **Pal** is positioned very close to the posterior border furrow and at the same distance from **G** as the center of **Pal**; the anterior margin is close to **G** and terminates at the level of its anterior margin. The highest point of **Pal** is lower than the highest point of **Bcl**. The palpebral ridges are almost untraceable.

The anterior and posterior branches of the facial sutures are very short; the anterior branches weakly converge, the posterior ones weakly diverge. The surface of **Cr** is smooth.

Comparison. The new species differs from *Irvingella norilica* Lazarenko, 1968 in having a strongly elongated **G** ($\mathbf{a_1G}$ is 1.54 of $\mathbf{b_3G}$), anterior two-thirds of which are semi-elliptical (anterior two-thirds of **G** are hemispherical in *I. norilica* ($\mathbf{a_1G}$ is subequal to $\mathbf{b_3G}$)) and in the longer **Bcl** (**bBcl** is 0.5 of $\mathbf{b_3G}$; whereas in *I. norilica*, **bBcl** is 0.31–0.40 of $\mathbf{b_3G}$).

The new species differs from *Irvingella perfecta* N. Tchernysheva, 1968 in having a longer and more convex **G**, the longitudinal profile of which is semicircular in its anterior part (it is weakly arcuate in *I. perfecta*) and in the **SO** originating from **SD** (**SO** is not touching **SD** in *I. perfecta*).

It differs from *Irvingella angustilimbata* Kobayashi, 1938 in having a larger **Cr**, strongly convex and elongated **G** (**G** is moderately convex and subquadrate in *I. angustilimbata*), in the absence of **A**, in the broader **Bcl** (**bBcl** is 0.5 of $\mathbf{b_3G}$, whereas **bBcl** is 0.4 of $\mathbf{b_3G}$ in *I. angustilimbata*), in the medial **Pal** (they are shifted anteriorly in *I. angustilimbata*), and in the palpebral ridges being indiscernible.

Distribution. Upper Cambrian, *Norilagnostus quadratus–Irvingella cipita* Zone.

Locality and Material. Ch-15-I-5: 1 **Cr** (well-preserved); Ch-18-10: 1 **Cr** (well-preserved) and 3 **Cr** (satisfactorily preserved).

Family Liostracinidae Raymond, 1937

Genus *Gibbura* Rosova et Varlamov, gen. nov.

Etymology. From the Latin *gibbus* (hump).

Type species. *Aplexura lepida* Lazarenko, 1968 (Lazarenko, 1968, p. 177, pl. 15, figs. 1–6). Northwestern Siberian Platform, Mokutei River, left tributary of

Plate 15

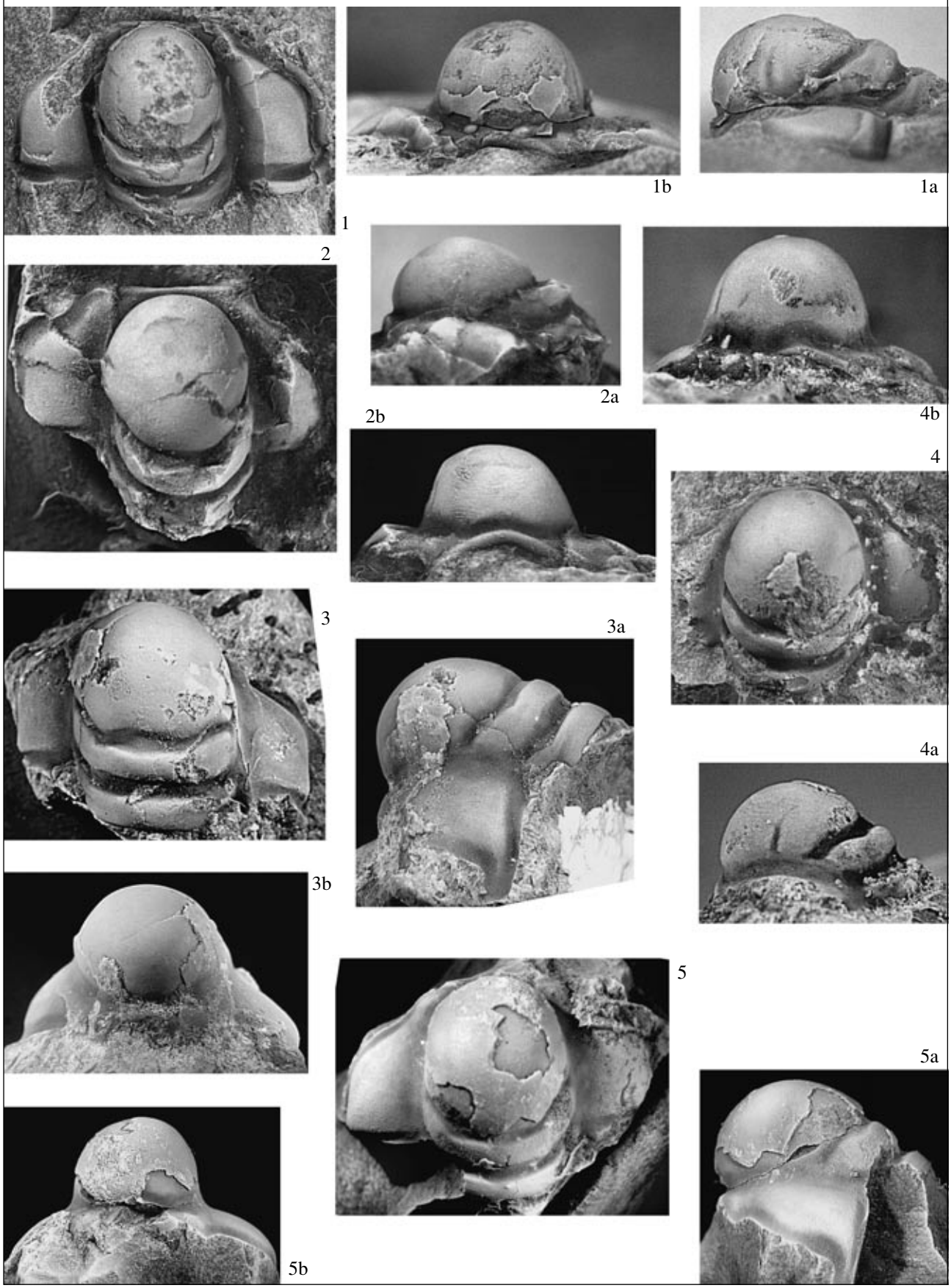

the Rybnaya River; Upper Cambrian, lower part of the *Amorphella* Zone.

Diagnosis. **Cr** small or medium-sized, transverse, with well-developed relief. **G** small, convex. **SD** in shape of surface bend. **SPg** concavely arcuate, distinct, extending slightly over **G** in front of palpebral ridges. Two pairs of **SG** in shape of short parallel, transverse or weakly oblique notches. **SO** very weakly saddle-shaped. **O** roughly triangular. **Cor** large (**a_1Cor** greater than **a_1G**), with relief—**Cp** developed in form of ball-like swelling, transforming through lowering surface into convex **Tm**. **Bcl** very broad (**bBcl** greater than **bG**), developed as triangular depression near **G** and elevated abaxially. **Pal** massive, weakly arcuate, shifted backward from **Cr** center. Palpebral ridges distinct, thick, long, oblique, closely adjacent to **G** interrupting **SD**. Anterior branches of facial sutures short, diverging before **Ar** and then turning inward. Posterior branches short, diverging. **Cr** surface unevenly covered with very large, scarce nodes, which arranged evenly only along **Ar** margin.

Species composition. Monotypic.

Comparison. On the one hand, this new genus is similar to the genus *Aplexura* Rosova from the stratotype of the Ensyan Horizon of the Upper Cambrian, and on the other hand, to the genus *Bolaspidina* N. Tchernysheva, which is known from the upper part of the Middle and the lower part of the Upper Cambrian (Tchernysheva, 1960, p. 242, pl. 53, figs. 6–8; Rosova, 1977, p. 67, pl. 4, figs. 19, 20 from the Tavgian Horizon of the Upper Cambrian; Ogienko and Garina, 2001, p. 198).

Gibbura gen. nov. differs from *Aplexura* Ros. (Rosova, 1963, p. 14) in having a very short **G**, weakly narrowing anteriorly, and a very large **Cor** (**a_1Cor** is greater than **a_1G**), with a ball-like swollen **Cp**, the palpebral ridges being very broad along their entire length, and in the tuberculate sculpture of **Cr**.

It differs from the genus *Bolaspidina* N. Tchernysheva in having a very short **G**, which weakly expands posteriorly or, sometimes, is subparallel-sided; the less distinct **SG**; extremely broad **Bcl** (**bBcl** is greater than **b_3G**); a more massive ball-like swollen **Cp** and in a different kind of the sculpture.

Remarks. Representatives of the genus *Gibbura* in the Norilsk District have been recorded in sections along the Mokutei River and the Mezhvilk Creek (left tributary of the Chopko River). It is difficult to say whether these finds come from the same stratigraphic level. Judging from the accompanying trilobite assemblage (Lazarenko, 1968, p. 179), beds in the section of the Mokutei River are somewhat older than beds along the Mezhvilk Creek.

Distribution. Northwestern Siberian Platform, Norilsk District, Mokutei River (left tributary of the Rybnaya River); Upper Cambrian, *Amorphella* Zone; Mezhvilk Creek (left tributary of Chopko River), Upper Cambrian, upper part of the Chopko Formation, beds with *Tukalandaspis egens.*

Gibbura lepida (Lazarenko, 1968)

Plate 16, figs. 6–8

Aplexura lepida Lazarenko, 1968: Lazarenko, 1968, p. 177, pl. 15, figs. 1–6.

Holotype. CSGM, no. 1/9654, **Cr**, figured by Lazarenko (1968, pl. 15, figs. 1–6); northwestern Siberian Platform, Mokutei River (left tributary of the Rybnaya River); Upper Cambrian, lower part of the *Amorphella* Zone.

Diagnosis. This is the only species in this genus.

Description. **Cr** is small or medium-sized (**a_1Cr** = 3–6 mm, **b_3Cr** = 4–9 mm), broadened (**b_3Cr** is approximately 1.3 of **a_1Cr**), with very prominent relief. **G** is small (**a_1G** is approximately 0.35 of **a_1Cr**), short (**a_1G** is approximately equal to **b_3G**), and convex. There are two pairs of **SG** in the shape of short parallel notches weakly beveled posteriorly. **G** weakly narrows forward until **S_2G**, then, weakly expands and merges with the palpebral ridges. The transverse profile of **G** is steeply arcuate. The sagittal profile is almost straight in the posterior two-thirds and arcuate downward in the anterior third. **SPg** is distinct, weakly concavely arcuate, slightly extended beyond **G** in the shape of foveate depressions in front of the inner ends of the palpebral ridges. **O** is triangular and convex. **SO** is weakly saddle-shaped or straight adaxially and directed forward abaxially. The highest point of **Cr** coincides with that of **G** and is slightly higher than the highest points of other elements of **Cr**.

Cor is large (**a_1Cor** is greater than **a_1G**), with prominent relief, subdivided into **Ar** and **A** (**a_1Ar** is approximately 0.6 of **a_1A**). **A** is subdivided into a cone-shaped swollen **Cp** and convex **Tm**. The highest point of **Tm** is shifted backward and outward from the center. **Ar** is weakly convex, parallel-sided, inclined toward **G** at 45°. The boundary between **A** and **Ar** is in the shape of a broad parallel-sided depression along its entire length. **Fix** are almost rectangular and broadened behind the palpebral ridges, in the shape of triangular depressions at the boundary with **G**, and abruptly ele-

Explanation of Plate 15

Figs. 1–5. *Irvingella cipita* Varlamov et Rosova sp. nov.: (1, 1a, 1b) holotype CSGM, no. 749/67, **Cr**, outcrop Ch-15-I-5, ×4.5; (1a) lateral view; (1b) frontal view; (2, 2a, 2b) specimen CSGM, no. 749/65, distorted **Cr**, outcrop Ch-18-10, ×4.5; (2a) lateral view, (2b) frontal view; (3, 3a, 3b) specimen CSGM, no. 749/60, distorted **Cr**, outcrop Ch-18-10, ×4; (3a) lateral view, (3b) frontal view; (4, 4a, 4b) specimen CSGM, no. 749/64, fragment of **Cr**, outcrop Ch-18-10, ×5; (4a) lateral view, (4b) frontal view; (5, 5a, 5b) specimen CSGM, no. 749/63, **Cr**, outcrop Ch-18-10, ×4.2; (5a) lateral view; (5b) frontal view.

All specimens from base of the *Norilagnostus quadratus–Irvingella cipita* Zone.

Plate 16

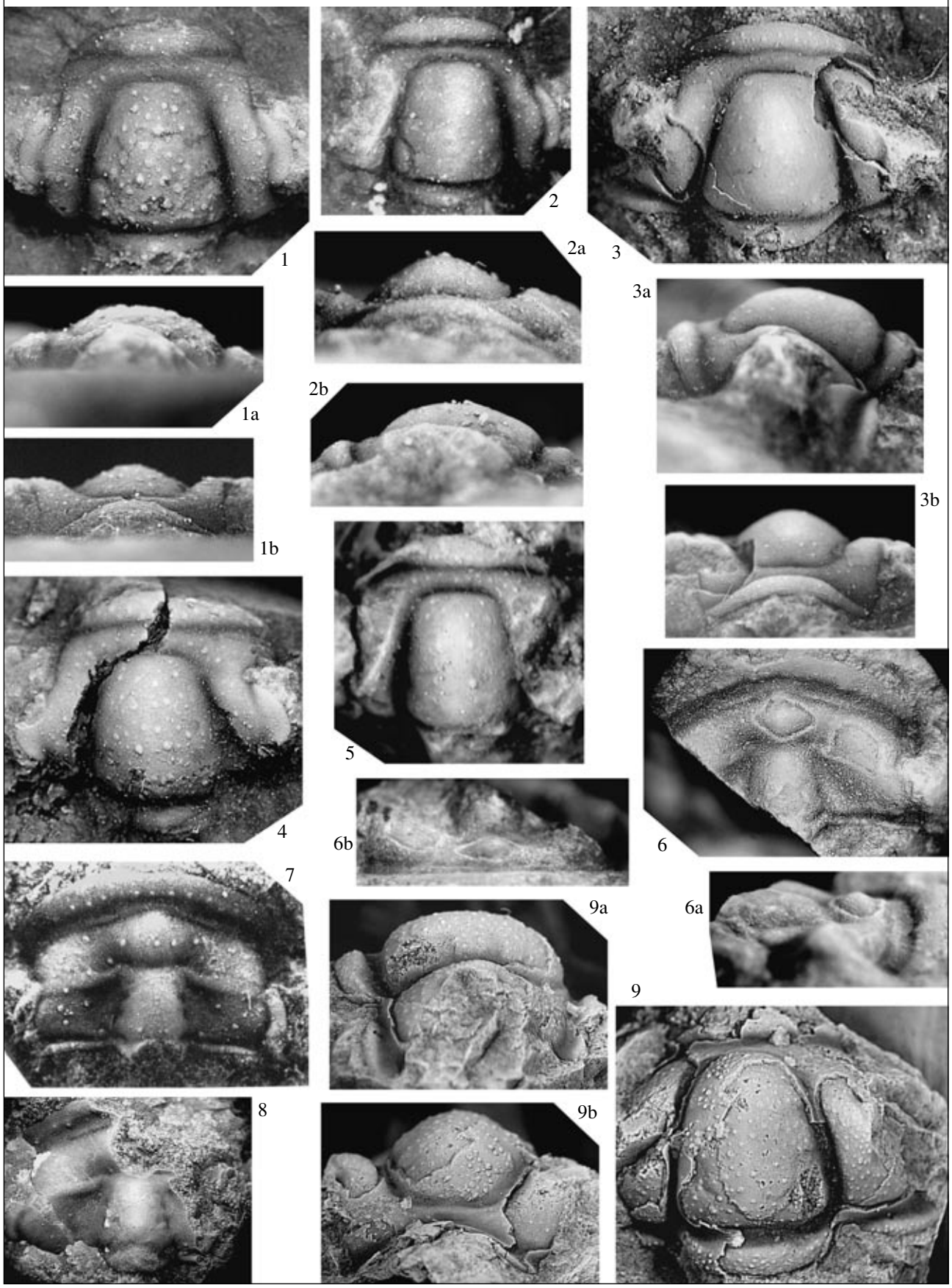

vated toward **Pal**. The posterior abaxial border is narrow, ridgelike, with a posteriorly directed outer end. **Pal** are small (**aPal** is approximately 0.75 of $\mathbf{a_1G}$) and weakly arcuate. The anterior margin of **Pal** is slightly anteriad of $\mathbf{S_2G}$. The palpebral ridges are distinct, straight, beveled forward from **Pal**. The anterior branches of the facial sutures are straight, weakly diverging at an angle of 20° to the axis of **Cr**. The posterior branches are short and divergent. The surface of **Cr** has an uneven pattern of very large and very scarce nodes. Along the posterior margin of **A**, nodes are of equal size and distributed evenly. Sometimes, a longitudinal arrangement of nodes is traceable on **Cor**, and a diagonal arrangement is traceable on **Bcl**.

Comparison. This is the only species in this genus.

Remarks. When comparing **Cr** from the Mezhvilk Creek with typical representatives of this species from the deposits of the Mokutei River, some dissimilarities in a number of morphological features of **Cr** and in the stratigraphic assignment are observable. Representatives from the Mokutei River are older than those from the Mezhvilk Creek. The lack of a complete collection of representatives of the genus **G**ibbura from the section along the Mezhvilk Creek prevents a confident assignment of morphological differences to intraspecific variability. Probably, two separate species of the genus Gibbura are involved.

Distribution. Northwestern Siberian Platform, Norilsk District, Mokutei River; Upper Cambrian, *Amorphella* Zone; Mezhvilk Creek (left tributary of the Chopko River); Upper Cambrian, beds with *Tukalandaspis egens.*

Locality and Material. **Ch-28-I-4b**: 3 **Cr** (well and poorly preserved).

Family incertae

Genus *Bijaspis* Petrunina, 1990

***Bijaspis nordica* Rosova et Makarova, sp. nov.**

Plate 16, figs. 1–5

Etymology. From the Latin *nord* (north).

Holotype. CSGM, no. 749/56, **Cr**; northwestern Siberian Platform, Norilsk District, Chopko River, Ch-11-I-3; Upper Cambrian, *Agnostotes* (*Pseudoglyptagnostus*) *clavatus–Irvingella perfecta* Zone, Chopko Formation (Pl. 16, fig. 1).

Diagnosis. **G** evenly narrowing anteriorly; **SAr** weakly arcuate backward, uniform along entire extent; **A** convex.

Description. **Cr** is small ($\mathbf{a_1Cr}$ = 1.8–3.5 mm), weakly transversely expanding ($\mathbf{a_1Cr}$ is 0.9 of $\mathbf{b_3Cr}$), moderately convex. The anterior and posterior margins of **Cr** are weakly arcuate. **G** is large ($\mathbf{a_1G}$ is 0.65 of $\mathbf{a_1Cr}$), truncate conical ($\mathbf{b_1G}$ is 0.6 of $\mathbf{b_5G}$). The sagittal profile of **G** is regularly weakly arcuate. The transverse profile of **G** is rounded triangular. Two or three pairs of weak **SG** originate from **SD**. $\mathbf{S_1G}$ are shallow, broad, geniculate. $\mathbf{S_2G}$ are shallower and shorter than $\mathbf{S_1G}$, and $\mathbf{S_3G}$ are barely noticeable. **SD** are distinct, deep, very narrow, sometimes slightly narrowing anteriorly, angularly transforming into a similarly broad but shallower **SPg**. **Cor** is small ($\mathbf{a_1Cor}$ is 0.3 of $\mathbf{a_1G}$), distinctly subdivided into a convex, lenslike **Ar** and a convex and narrow **A** ($\mathbf{a_1Ar}$ is greater than, or equal to $\mathbf{a_1A}$). The highest point of **Ar** is lower than the highest point of **G** and is almost at the same level as the highest point of **A**. **SAr** is weakly arcuate backward. **Tm** are abruptly inclined to the anterolateral corners **Cr**. **Bcl** are convex (**bBcl** is approximately 0.3 of $\mathbf{b_3G}$), inclined to **G** at an angle of 45°. The highest point of **Bcl** is near **SPal**, slightly lower than the highest point of **G**. The posterior part of **Fix** is relatively small, inclined outward. **SPal** are slightly narrower and shallower than **SD**. **Pal** are large (**aPal** is 0.5 of $\mathbf{a_1G}$, **bPal** is approximately 0.5 of **bBcl**), medial or slightly shifted posteriorly, weakly curved, almost parallel to the sagittal line of **Cr**. The highest point of **Pal** is lower than the highest point of **G**. The palpebral ridges are not traceable. Adaxially, **SO** is weakly arcuate backward, as deep as but broader than **SD**, abaxially narrowing. In general, **O** is very narrow, broadened in the middle ($\mathbf{a_1O}$ is 0.16 of $\mathbf{a_1G}$), sometimes with a small node; the highest point of **O** is lower than the highest point of **G**. The anterior branches of the facial sutures are almost parallel to each other; the posterior branches diverge diagonally. The surface of **Cr** is unevenly tuberculate, **G** is unevenly covered

Explanation of Plate 16

Figs. 1–5. *Bijaspis nordica* Rosova et Makarova sp. nov.: (1, 1a, 1b) holotype CSGM, no. 749/56, **Cr**, outcrop Ch-11-I-3, ×13; (1a) lateral view, ×15; (1b) frontal view, ×14; (2, 2a, 2b) specimen CSGM, no. 749/54, **Cr**, outcrop Ch-11-I-3, ×25; (2a) frontal view, ×24; (2b) lateral view, ×25; (3, 3a, 3b) specimen CSGM, no. 749/57, **Cr**, outcrop Ch-11-I-4, ×11; (3a) lateral view, ×15; (3b) frontal view, ×13; (4) specimen CSGM, no. 749/58, **Cr**, outcrop Ch-11-I-4, ×19; (5) specimen CSGM, no. 749/53, fragment of **Cr**, outcrop Ch-11-I-4, ×21.

Figs. 6–8. *Gibbura lepida* (Lazarenko) gen. nov.: (6, 6a, 6b) specimen CSGM, no. 749/34, incomplete **Cr**, outcrop Ch-28-I-4b, ×7; (6a) lateral view; (6b) frontal view; (7) specimen CSGM, no. 749/68, **Cr**, outcrop Ch-28-I-4b, ×10; (8) specimen CSGM, no. 749/66, fragment of **Cr**, outcrop Ch-28-I-4b, ×8.

Fig. 9. *Convexocephalus granularis* Varlamov sp. nov., specimen CSGM, no. 749/52, incomplete **Cr**, outcrop Ch-24-II-1, ×6: (9a) lateral view, (9b) frontal view.

Figs. 1–4. Specimens from the *Agnostotes* (*P.*) *clavatus–Irvingella perfecta* Zone. Figs. 6–8. Specimens from the beds with *Tukalandaspis egens.*

Fig. 9. Specimen from the *Irvingella norilica* Zone.

Plate 17

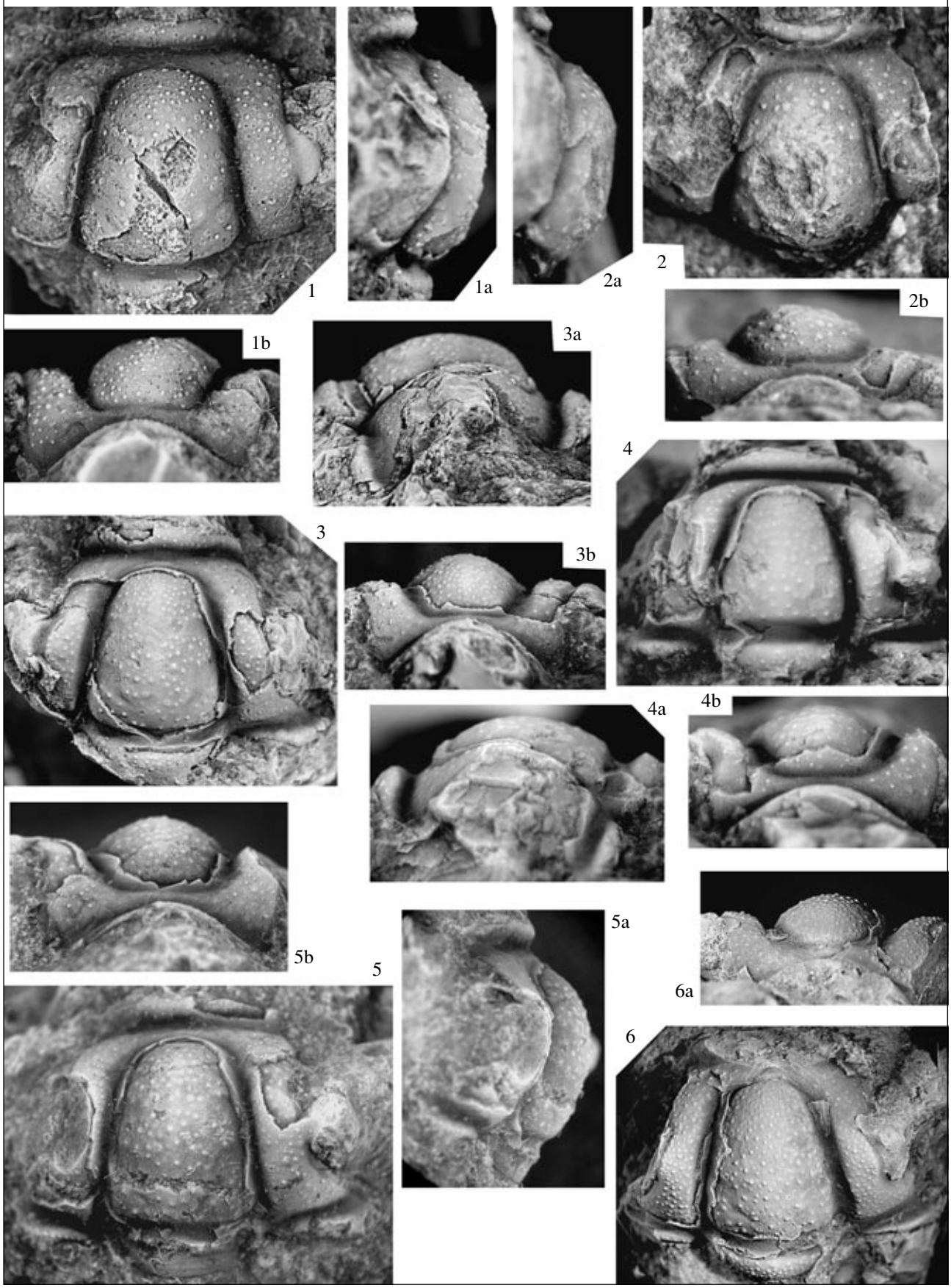

with nodes of different sizes, **Bcl** and **Cor** are covered with smaller uniform nodes, **Pal** are smooth.

Variability. Variable are the size of **A** (from $\mathbf{a_1A}$ equal to 0.5 of $\mathbf{a_1Ar}$ to $\mathbf{a_1A}$ approximately equal to $\mathbf{a_1Ar}$), the position of **Ar** in relation to **A** (the highest point of **Ar** is slightly higher, slightly lower than, or at the same level as the highest point of **A**), the degree of curvature of **Sar**, and the sculpture pattern of the **Cr** surface, being covered with scarce small nodes to closely spaced medium-sized nodes.

Comparison. The new species differs from the type species *Bijaspis krivtchikovi* Petrunina (Petrunina, 1990, p. 50) in the absence of a constriction at anterior one-third of $\mathbf{a_1G}$, in the **SAr** being straight or weakly arcuate backward and almost uniform along its entire length (in *B. krivtchikovi*, **SAr** is shallower adaxially and weakly arcuate forward), in the convex **A** (**A** is almost flat in *B. krivtchikovi*), the longer **Pal**, with **aPal** equal to 0.5 of $\mathbf{a_1G}$ (in *B. krivtchikovi*, **aPal** is approximately equal to 0.35 of $\mathbf{a_1G}$), and in untraceable palpebral ridges.

It is most similar to *Bijaspis katuniana* Petrunina (Petrunina, 1990, p. 51), but differs from it in the less expressed **SG**, straight or weakly arcuate backward **SAr** (**SAr** is weakly arcuate forward in *B. katuniana*), and in the untraceable palpebral ridges.

Distribution. Upper Cambrian, *Agnostotes* (*Pseudoglyptagnostus*) *clavatus–Irvingella perfecta* Zone.

Locality and Material. Ch-11-I-3: 3 **Cr** (well-preserved); Ch-11-I-4: 3 **Cr** (well-preserved).

Genus *Convexocephalus* Varlamov, gen. nov.

Etymology. From the Latin *convexus* (convex) and the *cephalon* (head).

Type species. *Convexocephalus granularis* Varlamov, sp. nov., northwestern Siberian Platform, Norilsk District, Chopko River; Upper Cambrian, *Agnostotes* (*Pseudoglyptagnostus*) *clavatus–Irvingella perfecta, Norilagnostus quadratus–Irvingella cipita* and *Irvingella norilica* zones.

Diagnosis. **Cr** medium-sized or large ($\mathbf{a_1Cr}$ = 8–18.5 mm), with prominent relief. **G** large ($\mathbf{a_1G}$ equal to 0.59–0.69 of $\mathbf{a_1Cr}$; $\mathbf{b_1G}$ approximately equal to 0.6 of $\mathbf{b_5G}$), gently narrowing forward, convex. Sagittal profile of **G** moderately arcuate, with highest point in center of **G** or shifted anteriorly. Transverse profile of **G** moderately arcuate. Two or three pairs of weakly expressed **SG** starting from **SD**. **SD** straight, medium-deep, broad or medium-broad, gently rounding anterolateral corners of **G** and sometimes terminating in small fossulae. **SPg** considerably shallower and narrower than **SD**, weakly traceable. **Cor** relatively small or medium-sized ($\mathbf{a_1Cor}$ approximately equal to 0.3–0.45 of $\mathbf{a_1G}$), distinctly subdivided into **A** and **Ar** ($\mathbf{a_1Ar}$ equal to or greater than $\mathbf{a_1A}$). **Ar** ridgelike, highest point of **Ar** higher than highest point of **A**, but lower than highest point of **G**. **A** flat or sulcate, sloping from **G** to **SAr**; **Tm** abruptly diagonally sloping from **G** and **Bcl** to anterolateral corners of **Cr**. **Bcl** medium-sized (**bBcl** equal to 0.37–0.40 of $\mathbf{b_3G}$), ascending almost vertically from **SD** in the first third of **bBcl**, then becoming subhorizontal. Highest point of **Bcl** lower than highest point of **G**. **Pal** small (**cPal** equal to 0.28–0.31 of $\mathbf{a_1G}$), curved, medial. Highest point of **Pal** almost at same level as highest point of **Bcl**. Adaxially, **SO** almost straight, broader but shallower than **SD**, narrowing abaxially and bending forward and downward. **O** broadened adaxially and narrowing abaxially. Anterior branches of facial sutures subparallel or weakly diverging, posterior branches diverging. **Cr** surface covered with closely spaced medium-sized nodes.

Comparison. The new genus differs from *Bijaspis* Petrunina (Petrunina, 1990, p. 49) in its larger dimensions ($\mathbf{a_1Cr}$ is 8–18.5 mm, whereas $\mathbf{a_1Cr}$ is 1.8–3.5 mm in *Bijaspis*), in having subquadrate **Cr** (**Cr** of *Bijaspis* slightly expands transversely), slightly narrowing forward **G**, (**G** is truncated conical in *Bijaspis*), flat **A** (**A** is convex in *Bijaspis*), **Ar** elevated over **A** (**Ar** are almost leveled to **A** in *Bijaspis*), **Bcl** more steeply inclined toward **SD** and in the shorter **Pal**, **aPal** is 0.28–0.31 of $\mathbf{a_1G}$ (**aPal** is 0.5 of $\mathbf{a_1G}$ in *Bijaspis*).

Distribution. Upper Cambrian, *Agnostotes* (*Pseudoglyptagnostus*) *clavatus–Irvingella perfecta, Norilagnostus quadratus–Irvingella cipita* and *Irvingella norilica* zones.

Convexocephalus granularis Varlamov, sp. nov.

Plate 16, fig. 9; Plate 17, figs. 1–6

Etymology. From the Latin *granularis* (granulated).

Holotype. CSGM, no. 749/44, **Cr**; northwestern Siberian Platform, Norilsk District, Chopko River, Ch-22a-II-1; Upper Cambrian, *Irvingella norilica* Zone, Chopko Formation (Pl. 17, fig. 1).

Explanation of Plate 17

Figs. 1–6. *Convexocephalus granularis* Varlamov sp. nov.: (1, 1a, 1b) holotype CSGM, no. 749/44, **Cr**, outcrop Ch-22a-II-1, ×5; (1a) lateral view; (1b) frontal view; (2, 2a, 2b) specimen CSGM, no. 749/48, incomplete **Cr**, outcrop Ch-11-I-3, ×10; (2a) lateral view, (2b) frontal view; (3, 3a, 3b) specimen CSGM, no. 749/47, **Cr** with exoskeleton remains, outcrop Ch-22a-II-1, ×5.5; (3a) lateral view; (3b) frontal view; (4, 4a, 4b) specimen CSGM, no. 749/62, incomplete **Cr**, outcrop Ch-11-I-3, ×5.5; (4a) lateral view; (4b) frontal view; (5, 5a, 5b) specimen CSGM, no. 749/45, incomplete **Cr**, outcrop Ch-22a-II-1, ×6; (5a) lateral view; (5b) frontal view; (6, 6a) specimen CSGM, no. 749/46, fragment of **Cr**, outcrop Ch-22a-II-1, ×3.5; (6a) frontal view.

Figs. 2 and 4. Specimens from the *Agnostotes* (*P.*) *clavatus–Irvingella perfecta* Zone. Figs. 1, 3–6. specimens from the *Irvingella norilica* Zone.

Diagnosis. **Cor** small (**a_1Cor** equal to 0.3 of **a_1G**). **SAr** as deep as but narrower than **SD**, arcuate backward. Boundary between **Ar** and **A** distinct. Posterior margin of **Ar** arcuate backward. **A** almost flat, sloping from **G** to **SAr**.

Description. **Cr** is medium-sized or large (**a_1Cr** is 9.5, that is, 8–14 mm), subquadrate (**a_1Cr** is almost equal to **b_3Cr**), with prominent relief. The anterior margin of **Cr** is almost straight.

G is large (**a_1G** is 0.59–0.69 of **a_1Cr**), weakly narrowing anteriorly (**b_1G** is 0.57–0.6 of **b_5G**), convex, with rounded anterolateral corners. The sagittal profile of **G** is moderately arcuate, with the highest point in the center of **G** or shifted anteriorly. The transverse profile of **G** is moderately arcuate. There are 2 or 3 pairs of weakly expressed **SG**, all of them start from **SD**. **S_1G** are long, oblique, weakly S-shaped. **S_2G** and **S_3G** are less distinct, short, straight, almost transverse. **SD** are straight, medium-deep and medium-broad, uniform along their entire length, being slightly shallower only near the anterolateral corners of **G**, sometimes terminating in small fossulae. **SPg** is considerably shallower and narrower than **SD**, poorly traceable.

Cor is relatively small (**a_1Cor** is 0.21–0.27 of **a_1G**), distinctly subdivided into **A** and **Ar**. **SAr** as deep as but slightly narrower than **SD**, arcuate backward. **Ar** and **A** are almost equal. **Ar** is ridgelike, its posterior margin is arcuate backward and steeply elevated over **A**. The almost flat **A** is inclined from **G** to **SAr**. The highest point of **Ar** is higher than the highest point of **A** and considerably lower than the highest point of **G**. **Tm** are abruptly, diagonally inclined from **G** and **Bcl** to the anterolateral corners of **Cr**.

Bcl are medium-sized (**bBcl** is 0.37–0.40 of **b_3G**), ascending almost vertically from **SD** in the first third of **bBcl**, then becoming flat and subhorizontal. The highest point of **Bcl** is in the center of **Bcl** or on the boundary with **Pal** and is considerably lower than the highest point of **G**. **Pal** are small (**aPal** is 0.28–0.31 of **a_1G**; **bPal** are almost 0.5 of **bBcl**), curved, medial. Due to the almost straight, subparallel outer margins of **Fix**, **Pal** strongly prominent project outward. The highest point of **Pal** is almost at the same level as the highest point of **Bcl**. **SPal** are broad, but narrower and shallower than **SD**.

SO is broader but shallower than **SD**, adaxially, almost straight or sometimes with a small bend forward, abaxially slightly narrowing and curving forward and downward. **O** is broadened adaxially (**a_1O** is 0.17–0.21 of **a_1G**), and narrowing abaxially. The posterior part of **Fix** is relatively small, approximately equal to 0.21 of **a_1G**, slightly extended abaxially. The posterior border of **Cr** is ridgelike, constituting 0.63 of **b_5G**, very narrow near **O**, broadening on the sides. The posterior border furrow expands abruptly and becomes shallower outward.

The anterior branches of facial sutures are almost parallel, the posterior branches diverge.

The surface of **Cr** on both a cast and the exoskeleton is evenly covered with numerous medium-sized, equal nodes.

Variability. **SD** varies from medium-broad to broad; the highest point of **Bcl** is situated in the middle of **Bcl** or at the boundary with **Pal**; the highest point of **Pal** is usually lower than the highest point of **Bcl**, but in some specimens, the highest point of **Pal** is at the same level as, or slightly higher than, the highest point of **Bcl**.

Comparison. This is the only species in the genus.

Remarks. Some specimens (Pl. 17, figs. 4, 5) were photographed from slightly below; therefore, on the photographs **SAr** of these specimens do not appear clearly arcuate backward as they are on the actual specimens.

Distribution. Upper Cambrian, *Agnostotes* (*Pseudoglyptagnostus*) *clavatus–Irvingella perfecta*, *Irvingella norilica* zones.

Locality and Material. Ch-11-I-3: 3 **Cr** (well-preserved); Ch-22a-II-1: 4 **Cr** (well-preserved); and Ch-24: 2 **Cr** (well-preserved) and 2 **Cr** (satisfactorily preserved).

ACKNOWLEDGMENTS

A.L. Makarova (SRIGGMR) was actively involved in describing a number of species. Photographs of trilobites were produced by A. Aleinikov.

REFERENCES

1. C. L. Chu, "Trilobites from the Kushan Formation of North and Northeastern China," Inst. Palaeontol. Acad. Sin. Mem., No. 2, 44–128 (1959).
2. V. A. Datsenko and N. P. Lazarenko, "Biostratigraphy of the Cambrian Beds of the Northwestern Siberian Platform," in *Biostratigraphy and Fauna of the Cambrian Beds of the Northwestern Siberian Platform*, Ed. by B. V. Tkachenko and N. N. Urvantsev (Nedra, Leningrad, 1968), pp. 7–117 [in Russian].
3. G. Kh. Ergaliev, *Trilobites from the Middle and Upper Cambrian of the Lesser Karatau* (Nauka Kaz. SSR, Alma-Ata, 1980) [in Russian].
4. N. P. Lazarenko, "Biostratigraphy and Some New Trilobites from the Upper Cambrian of the Olenek Uplift and Kharaulakh Mountains," Uch. Zap. NIIGA., No. 11 (Paleontology and Biostratigraphy), 33–78 (1966).
5. N. P. Lazarenko, "New Trilobites from the Cambrian Beds of Northern Siberia," in *Biostratigraphy and Fauna of the Cambrian Beds of the Northwestern Siberian Platform*, Ed. by B. V. Tkachenko and N. N. Urvantsev (Nedra, Leningrad, 1968), pp. 176–203 [in Russian].
6. E. V. Lermontova, "Class Trilobites," in *Atlas of the Guiding Taxa of Extinct Faunas of the USSR*, Ed. by A. G. Vologdin (Gosgeolizdat, Moscow–Leningrad, 1940), pp. 112–157 [in Russian].
7. Y. H. Lu and H. L. Lin, "The Cambrian Trilobites of Western Zhejiang," Paleontol. Sin., Ser. B, No. 25 (178), 1–273 (1989).

8. L. V. Ogienko and S. Yu. Garina, *Stratigraphy and Trilobites of the Cambrian of the Siberian Platform* (Nauchn. Mir, Moscow, 2001) [in Russian].
9. A. A. Öpik, "The Mindyallan Fauna of North-Western Queensland: V. 1: Text, V. 2: Appendixes, Plates and Index," BMR Bull., No. 74, Part 1, 1–404; Part 2, 1–166 (1967).
10. A. R. Palmer, "*Glyptagnostus* and Associated Trilobites in the United States," Geol. Surv. Prof. Pap., Washington US Govt. Print. Off., No. 374-F, 1–50 (1962).
11. A. R. Palmer, "Trilobites of the Late Cambrian Pterocephaliid Biomere in the Great Basin, United States," Geol. Surv. Prof. Pap., Washington US Govt. Print. Off., No. 493, 1–106 (1965).
12. Shanchi Peng, "Upper Cambrian Biostratigraphy and Trilobite Faunas of the Cili-Taoyuan Area, Northwestern Hunan, China," Assoc. Australas. Palaeontol. Mem., No. 13, 1–119 (1992).
13. Z. E. Petrunina, "Some New Early Ordovician Trilobites of the Western Part of the Altai–Sayan Mountain Region," in *News in Paleontology and Biostratigraphy of the Paleozoic of the Asian Part of the USSR* (Nauka, Novosibirsk, 1990), pp. 21–58 [in Russian].
14. B. R. Pratt, "Trilobites of the Marjuman and Steptoen Stages (Upper Cambrian), Rabbitkettle Formation, Southern Mackenzie Mountains, Northwest Canada," Palaeontogr. Canad., No. 9, 1–180 (1992).
15. A. V. Rosova, "Biostratigraphic Chart of the Zonation of the Upper Cambrian and the Terminal Middle Cambrian of the Northwestern Siberian Platform and New Upper Cambrian Trilobites from the Kulyumbe River," Geol. Geofiz., No. 9, 3–19 (1963).
16. A. V. Rosova, *Biostratigraphy and Description of Trilobites from the Middle and Upper Cambrian of the Northwestern Siberian Platform* (Nauka, Moscow, 1964) [in Russian].
17. A. V. Rosova, *Biostratigraphy and Trilobites from the Upper Cambrian and Lower Ordovician of the Northwestern Siberian Platform* (Nauka, Moscow, 1968) [in Russian].
18. A. V. Rosova, "On the Biostratigraphic Charts of the Upper Cambrian and Lower Ordovician of the Northwestern Siberian Platform," Geol. Geofiz., No. 5, 26–31 (1970).
19. J. H. Shergold, "Late Cambrian and Early Ordovician Trilobites from the Burke River Structural Belt, Western Queesland, Australia," BMR Bull., No. 153, Part 1 (Text), Part 2 (Plates), 1–251 (1975).
20. J. H. Shergold, "Classification of the Trilobite *Pseudagnostus*," Palaeontology, No. 20, 69–100 (1977).
21. Xiaowen Sun, "Cambrian Agnostids from the North China Platform," Palaeontol. Cathayana, No. 4, 53–99 (1989).
22. N. E. Tchernysheva, "Class Trilobita," in *New Species of Ancient Plants and Invertebrates of the USSR: Part 2* (Gosgeoltekhizdat, Moscow, 1960), pp. 211–255 [in Russian].
23. N. E. Tchernysheva, "A New Species of *Irvingella* (a Cambrian Trilobite)," in *Biostratigraphy and Fauna of the Cambrian Beds of the Northwestern Siberian Platform*, Ed. by B. V. Tkachenko and N. N. Urvantsev (Nedra, Leningrad, 1968), pp. 203–211 [in Russian].
24. A. I. Varlamov, K. L. Pak, and A. V. Rosova, "The Upper Cambrian of the Chopko River Section, Norilsk Region, Northwestern Siberian Platform: Stratigraphy and Trilobites," Paleontol. J., No. **40** (1 Suppl.), S1–S56 (2006).
25. H. B. Whittington and S. R. A. Kelly, "Morphological Terms Applied to Trilobita," in *Treatise on Invertebrate Paleontology: Part O. Arthropoda 1: Trilobita, Revised*, Ed. by R. L. Kaesler (Univ. Kansas Press, Kansas, 1997), pp. 313–329.
26. J. L. Wilson, "Revisions in Nomenclature and New Species of Cambro–Ordovician Trilobites from the Marathon Uplift, West Texas," J. Paleontol. **30** (6), 1341–1349 (1956).